3GPP TR 36.873 V12.7.0 (2017-12)

Technical Report

3rd Generation Partnership Project;
Technical Specification Group Radio Access Network;
Study on 3D channel model for LTE
(Release 12)

Keywords
<LTE, radio, model>

3GPP

Postal address

3GPP support office address
650 Route des Lucioles - Sophia Antipolis
Valbonne - FRANCE
Tel.: +33 4 92 94 42 00 Fax: +33 4 93 65 47 16

Internet
http://www.3gpp.org

Contents

Foreword

This Technical Report has been produced by the 3rd Generation Partnership Project (3GPP).

The contents of the present document are subject to continuing work within the TSG and may change following formal TSG approval. Should the TSG modify the contents of the present document, it will be re-released by the TSG with an identifying change of release date and an increase in version number as follows:

Version x.y.z

where:

x the first digit:

1 presented to TSG for information;

2 presented to TSG for approval;

3 or greater indicates TSG approved document under change control.

y the second digit is incremented for all changes of substance, i.e. technical enhancements, corrections, updates, etc.

z the third digit is incremented when editorial only changes have been incorporated in the document.

1 Scope

The present document captures the findings of the study item "Study on 3D-channel model for Elevation Beamforming and FD-MIMO studies for LTE" [3] and aims to help TSG RAN WG1 to properly model and evaluate the performance of physical layer techniques using 3D channel models.

This document relates to the 3GPP evaluation methodology and covers the modelling of the physical layer of both Mobile Equipment (ME) and Access Network (AN) of 3GPP systems.

It intends to capture the scenarios relevant to 3D channel models and the modifications to the 3GPP evaluation methodology needed to support 3D channel modelling.

2 References

The following documents contain provisions which, through reference in this text, constitute provisions of the present document.

- References are either specific (identified by date of publication, edition number, version number, etc.) or non-specific.
- For a specific reference, subsequent revisions do not apply.
- For a non-specific reference, the latest version applies. In the case of a reference to a 3GPP document (including a GSM document), a non-specific reference implicitly refers to the latest version of that document *in the same Release as the present document*.

[1] 3GPP TR 21.905: "Vocabulary for 3GPP Specifications".

[2] RP-122034: Work Item Description for "Study on 3D-channel model for Elevation Beamforming and FD-MIMO studies for LTE".

[3] RP-130811: Revised Work Item Description for "Study on 3D-channel model for Elevation Beamforming and FD-MIMO studies for LTE".

[4] 3GPP TR 36.814 (V9.0.0): "Further Advancements for E-UTRA, Physical Layer Aspects".

[5] ITU-R Rec. P.1816: "The prediction of the time and the spatial profile for broadband land mobile services using UHF and SHF bands"

[6] R1-140765: "Polarized antenna modelling" Ericsson, RAN1#76, Feb 2014.

[7] R1-140842: "Discussions on Wrapping Methodology" Ericsson, RAN1#76, Feb 2014.

[8] R1-140843: "Summary of Phase-1 and Phase-2 calibration results from [75-29]", NSN, Nokia, RAN1#76, Feb 2014.

[9] 3GPP TR 25.996: "Spatial channel model for Multiple Input Multiple Output (MIMO) simulations".

[10] R1-143469: "Summary of 3D channel model calibration results", Nokia Networks, Nokia Corporation, RAN1#78, Aug 2014.

[11] R1-140972: "WF on Channel Modeling for High Rise Scenario", Alcatel-Lucent, Alcatel-Lucent Shanghai Bell, CATR, CATT, CHTTL, CMCC, Huawei, HiSilicon, Hitachi, INTEL, LGE, NEC, NTT DoCoMo, Samsung, ZTE, RAN1#76, Feb 2014.

[12] R1-140600: "Measurement and Discussions on Small Scale Parameters for High Rise Scenario", CMCC, RAN1#76, Feb 2014.

[13] R1-140284: "Discussion on channel model for high rise scenario", ZTE, RAN1#76, Feb 2014.

[14] R1-140204: "Details of channel modeling for high rise scenario", Huawei, HiSilicon, RAN1#76, Feb 2014.

[15] R1-140770: "Modelling Considerations for the High-Rise Scenario", Ericsson, RAN1#76, Feb 2014.

[16] IST-WINNER II Deliverable 1.1.2 v.1.2, "WINNER II Channel Models", IST-WINNER2, Tech. Rep., 2007 (http://www.ist-winner.org/deliverables.html).

3 Definitions and abbreviations

3.1 Definitions

For the purposes of the present document, the terms and definitions given in TR 21.905 [1] and the following apply.
A term defined in the present document takes precedence over the definition of the same term, if any, in TR 21.905 [1].

3.2 Abbreviations

For the purposes of the present document, the abbreviations given in TR 21.905 [1] and the following apply.
An abbreviation defined in the present document takes precedence over the definition of the same abbreviation, if any, in TR 21.905 [1].

FD-MIMO	Full Dimension MIMO
GCS	Global Coordinate System
LCS	Local Coordinate System

4 Introduction

At 3GPP TSG RAN #58 meeting the Study Item Description on "Study on 3D-channel model for Elevation Beamforming and FD-MIMO studies for LTE" was approved [2], which was subsequently revised at RAN#60 [3].

This study item covers the identification of scenarios applicable to 3D beamforming, FD-MIMO and the evaluation methodology needed for modelling and evaluation of such techniques. This TR documents the modified evaluation methodology including 3D channel models needed for studying the above techniques.

5 General

5.1 Coordinate system

5.1.1 Definition

A coordinate system is defined by the x, y, z axes, the spherical angles and the spherical unit vectors as shown in Figure 5.1.1.

Figure 5.1.1 defines the zenith angle θ and the azimuth angle ϕ in a Cartesian coordinate system.

Note that $\theta = 0$ points to the zenith and $\theta = 90^0$ points to the horizon.

The field component in the direction of $\hat{\theta}$ is given by F_θ and the field component in the direction of $\hat{\phi}$ is given by F_ϕ.

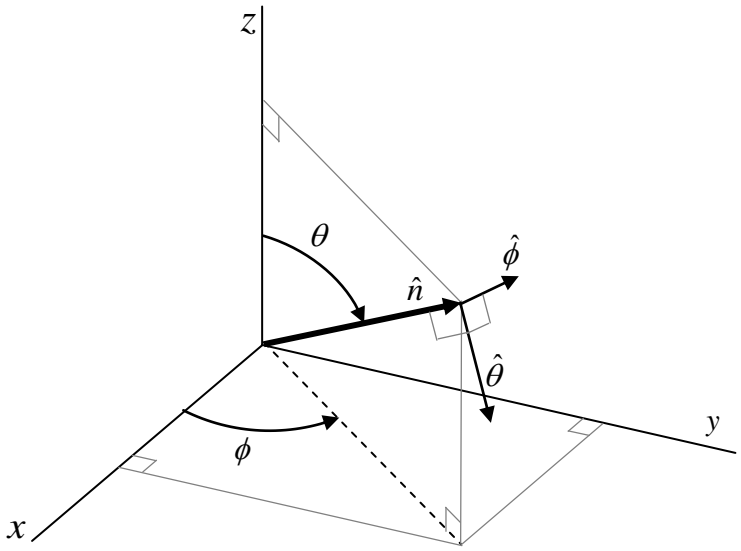

Figure 5.1.1: Definition of spherical angles and spherical unit vectors in a Cartesian coordinate system, where $\hat{n}$ is the given direction, $\hat{\theta}$ and $\hat{\phi}$ are the spherical basis vectors

5.1.2 Local and global coordinate systems

A Global Coordinate System (GCS) is defined for a system comprising of multiple BSs and UTs. An antenna array for a BS or a UT can be defined in a Local Coordinate System (LCS). An LCS is used as a reference to define the vector far-field that is pattern and polarization, of each antenna element in an array. It is assumed that the far-field is known in the LCS by formulae. The placement of an array within the GCS is defined by the translation between the GCS and a LCS. The orientation of the array with respect to the GCS is defined in general by a sequence of rotations (described in clause 5.1.3). Since this orientation is in general different from the GCS orientation, it is necessary to map the vector fields of the array elements from the LCS to the GCS. This mapping depends only on the orientation of the array and is given by

the equations in clause 5.13.
Note that any arbitrary mechanical orientation of the array can be achieved by rotating the LCS with respect to the GCS.

5.1.3 Transformation from a LCS to a GCS

A GCS with coordinates (x, y, z, θ, ϕ) and unit vectors ($\hat{\theta}$, $\hat{\phi}$) and an LCS with "primed" coordinates (x', y', z', θ', ϕ') and "primed" unit vectors ($\hat{\theta}'$, $\hat{\phi}'$) are defined with a common origins in Figures 5.1.3-1 and 5.1.3-2. Figure 5.1.3-1 illustrates the sequence of rotations that relate the GCS (gray) and the LCS (blue).
Figure 5.1.3-2 shows the coordinate direction and unit vectors of the GCS (gray) and the LCS (blue).
Note that the vector fields of the antenna array elements are defined in the LCS. In Figure 5.1.3-1 we consider an arbitrary 3D-rotation of the LCS with respect to the GCS given by the angles α, β, γ. The set of angles α, β, γ can also be termed as the orientation of the antenna array with respect to the GCS.
Note that the transformation from a LCS to a GCS depends only on the angles α, β, γ. The angle α is called the bearing angle, β is called the downtilt angle and γ is called the slant angle.

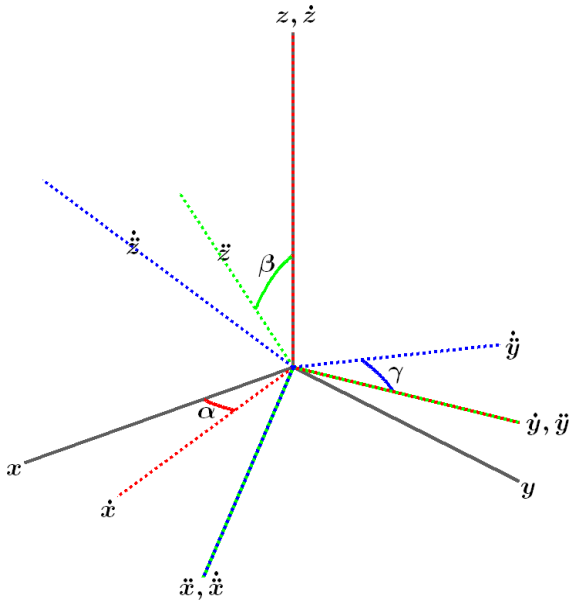

Figure 5.1.3-1: Orienting the LCS (blue) with respect to the GCS (gray) by a sequence of 3 rotations: α, β, γ.

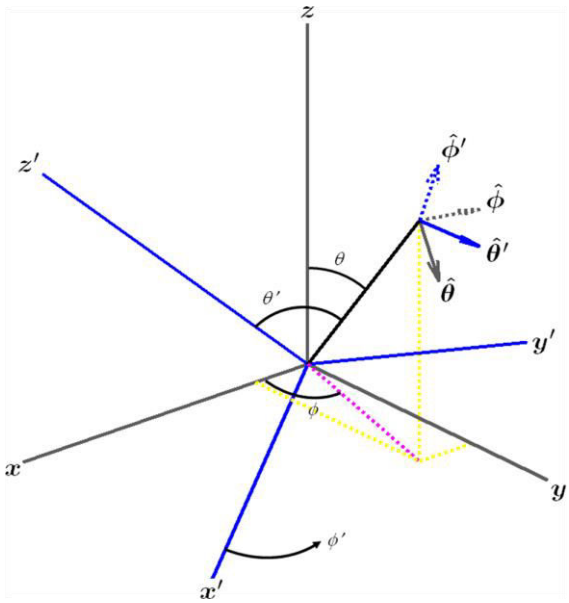

Figure 5.1.3-2: Definition of spherical coordinates and unit vectors in both the GCS and LCS.

Let $A'(\theta',\phi')$ denote an antenna element pattern in the LCS and $A(\theta,\phi)$ denote the same antenna element pattern in the GCS. Then the two are related simply by

$$A(\theta,\phi) = A'(\theta',\phi') \tag{5.1-1}$$

with θ' and ϕ' given by (5.1-7) and (5.1-8).

Let us denote the polarized field components in the LCS by $F_{\theta'}(\theta',\phi')$, $F_{\phi'}(\theta',\phi')$ and in the GCS by $F_{\theta}(\theta,\phi)$, $F_{\phi}(\theta,\phi)$. Then they are related by equation (5.1-11).

Any arbitrary 3-D rotation can be specified by at most 3 elemental rotations, and following the framework of Figure 5.1.3-1, a series of rotations about the z, $\dot{y}$ and $\ddot{x}$ axes are assumed here, in that order.
The dotted and double-dotted marks indicate that the rotations are intrinsic, which means that they are the result of one (·) or two (··) intermediate rotations. In other words, the $\dot{y}$ axis is the original y axis after the first rotation about z, and the $\ddot{x}$ axis is the original x axis after the first rotation about z and the second rotation about $\dot{y}$.
A first rotation of α about z sets the antenna bearing angle (i.e. the sector pointing direction for a BS antenna element).

The second rotation of β about $\dot{y}$ sets the antenna downtilt angle.

Finally, the third rotation of γ about $\ddot{x}$ sets the antenna slant angle.

The orientation of the *x*, *y* and *z* axes after all three rotations can be denoted as $\dddot{x}$, $\dddot{y}$ and $\dddot{z}$.

These triple-dotted axes represents the final orientation of the LCS, and for notational purposes denoted as the *x′*, *y′* and *z′* axes (local or "primed" coordinate system).

In order to establish the equations for transformation of the coordinate system and the polarized antenna field patterns between the GCS and the LCS, it is necessary to determine the composite rotation matrix that describes the transformation of point (*x*, *y*, *z*) in the GCS into point (*x′*, *y′*, *z′*) in the LCS.

This rotation matrix is computed as the product of three elemental rotation matrices.

The matrix to describe rotations about the *z*, $\dot{y}$ and $\ddot{x}$ axes by the angles α, β and γ respectively and in that order is defined in equation (5.1-2).

$$R = R_Z(\alpha)R_Y(\beta)R_X(\gamma) = \begin{pmatrix} +\cos\alpha & -\sin\alpha & 0 \\ +\sin\alpha & +\cos\alpha & 0 \\ 0 & 0 & 1 \end{pmatrix}\begin{pmatrix} +\cos\beta & 0 & +\sin\beta \\ 0 & 1 & 0 \\ -\sin\beta & 0 & +\cos\beta \end{pmatrix}\begin{pmatrix} 1 & 0 & 0 \\ 0 & +\cos\gamma & -\sin\gamma \\ 0 & +\sin\gamma & +\cos\gamma \end{pmatrix} \tag{5.1-2}$$

The reverse transformation is given by the inverse of R, which is also equal to the transpose of R since it is orthogonal.

$$R^{-1} = R_X(-\gamma)R_Y(-\beta)R_Z(-\alpha) = R^T \tag{5.1-3}$$

The simplified forward and reverse composite rotation matrices are given in equations (5.1-4) and (5.1-5).

$$R = \begin{pmatrix} \cos\alpha\cos\beta & \cos\alpha\sin\beta\sin\gamma - \sin\alpha\cos\gamma & \cos\alpha\sin\beta\cos\gamma + \sin\alpha\sin\gamma \\ \sin\alpha\cos\beta & \sin\alpha\sin\beta\sin\gamma + \cos\alpha\cos\gamma & \sin\alpha\sin\beta\cos\gamma - \cos\alpha\sin\gamma \\ -\sin\beta & \cos\beta\sin\gamma & \cos\beta\cos\gamma \end{pmatrix} \tag{5.1-4}$$

$$R^{-1} = \begin{pmatrix} \cos\alpha\cos\beta & \sin\alpha\cos\beta & -\sin\beta \\ \cos\alpha\sin\beta\sin\gamma - \sin\alpha\cos\gamma & \sin\alpha\sin\beta\sin\gamma + \cos\alpha\cos\gamma & \cos\beta\sin\gamma \\ \cos\alpha\sin\beta\cos\gamma + \sin\alpha\sin\gamma & \sin\alpha\sin\beta\cos\gamma - \cos\alpha\sin\gamma & \cos\beta\cos\gamma \end{pmatrix} \tag{5.1-5}$$

These transformations can be used to derive the angular and polarization relationships between the two coordinate systems.

In order to establish the angular relationships, consider a point (*x*, *y*, *z*) on the unit sphere defined by the spherical coordinates (ρ=1, θ, ϕ), where ρ is the unit radius, θ is the zenith angle measured from the +*z*-axis, and ϕ is the azimuth angle measured from the +*x*-axis in the *x*-*y* plane. The Cartesian representation of that point is given by

$$\hat{\rho} = \begin{pmatrix} x \\ y \\ z \end{pmatrix} = \begin{pmatrix} \sin\theta\cos\phi \\ \sin\theta\sin\phi \\ \cos\theta \end{pmatrix} \tag{5.1-6}$$

The zenith angle is computed as $\arccos(\hat{\rho}\cdot\hat{z})$ and the azimuth angle as $\arg(\hat{x}\cdot\hat{\rho} + j\,\hat{y}\cdot\hat{\rho})$, where $\hat{x}$, $\hat{y}$ and $\hat{z}$ are the Cartesian unit vectors. If this point represents a location in the GCS defined by θ and ϕ, the corresponding position in the LCS is given by $R^{-1}\hat{\rho}$, from which local angles θ' and ϕ' can be computed. The results are given in equations (5.1-7) and (5.1-8).

$$\theta'(\alpha,\beta,\gamma;\theta,\phi) = \arccos\left(\begin{bmatrix} 0 \\ 0 \\ 1 \end{bmatrix}^T R^{-1}\hat{\rho}\right) = \text{acos}\left(\cos\beta\cos\gamma\cos\theta + \left(\sin\beta\cos\gamma\cos(\phi-\alpha) - \sin\gamma\sin(\phi-\alpha)\right)\sin\theta\right) \tag{5.1-7}$$

$$\phi'(\alpha,\beta,\gamma;\theta,\phi)=\arg\left(\begin{bmatrix}1\\ j\\ 0\end{bmatrix}^T R^{-1}\hat{\rho}\right)=\arg\begin{pmatrix}(\cos\beta\sin\theta\cos(\phi-\alpha)-\sin\beta\cos\theta)+\\ j(\cos\beta\sin\gamma\cos\theta+(\sin\beta\sin\gamma\cos(\phi-\alpha)+\cos\gamma\sin(\phi-\alpha))\sin\theta)\end{pmatrix} \quad (5.1\text{-}8)$$

These formulae relate the spherical angles (θ, ϕ) of the GCS to the spherical angles (θ', ϕ') of the LCS given the rotation operation defined by the angles (α, β, γ).

Let us denote the polarized field components $F_\theta(\theta,\phi)$, $F_\phi(\theta,\phi)$ in the GCS and $F_{\theta'}(\theta',\phi')$, $F_{\phi'}(\theta',\phi')$ in the LCS. Then they can be related by

$$\begin{pmatrix}F_\theta(\theta,\phi)\\ F_\phi(\theta,\phi)\end{pmatrix}=\begin{pmatrix}\hat{\theta}(\theta,\phi)^T R\hat{\theta}'(\theta',\phi') & \hat{\theta}(\theta,\phi)^T R\hat{\phi}'(\theta',\phi')\\ \hat{\phi}(\theta,\phi)^T R\hat{\theta}'(\theta',\phi') & \hat{\phi}(\theta,\phi)^T R\hat{\phi}'(\theta',\phi')\end{pmatrix}\begin{pmatrix}F_{\theta'}(\theta',\phi')\\ F_{\phi'}(\theta',\phi')\end{pmatrix} \quad (5.1\text{-}9)$$

In this equation, $\hat{\theta}$ and $\hat{\phi}$ represent the spherical unit vectors of the GCS, and $\hat{\theta}'$ and $\hat{\phi}'$ are the representations in the LCS. The forward rotation matrix R transforms the LCS unit vectors into the GCS frame of reference.
These pairs of unit vectors are orthogonal and can be represented as shown in Figure 5.1.3-3.

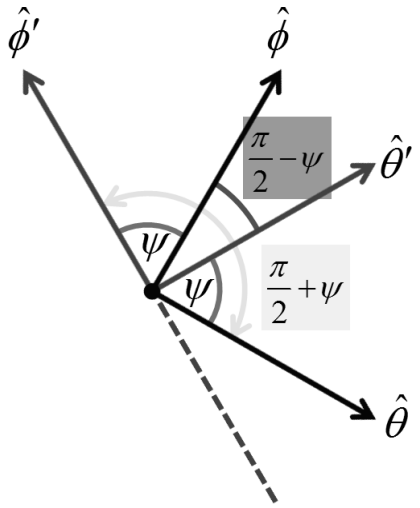

Figure 5.1.3-3: Rotation of the spherical basis vectors by an angle ψ due to the orientation of the LCS with respect to the GCS

Assuming an angular displacement of ψ between the two pairs of unit vectors, the rotation matrix of equation (5.1-9) can be further simplified as:

$$\begin{pmatrix}\hat{\theta}(\theta,\phi)^T R\hat{\theta}'(\theta',\phi') & \hat{\theta}(\theta,\phi)^T R\hat{\phi}'(\theta',\phi')\\ \hat{\phi}(\theta,\phi)^T R\hat{\theta}'(\theta',\phi') & \hat{\phi}(\theta,\phi)^T R\hat{\phi}'(\theta',\phi')\end{pmatrix}=\begin{pmatrix}\cos\psi & \cos(\pi/2+\psi)\\ \cos(\pi/2-\psi) & \cos\psi\end{pmatrix}=\begin{pmatrix}+\cos\psi & -\sin\psi\\ +\sin\psi & +\cos\psi\end{pmatrix} \quad (5.1\text{-}10)$$

and equation (5.1-9) can be written as:

$$\begin{pmatrix}F_\theta(\theta,\phi)\\ F_\phi(\theta,\phi)\end{pmatrix}=\begin{pmatrix}+\cos\psi & -\sin\psi\\ +\sin\psi & +\cos\psi\end{pmatrix}\begin{pmatrix}F_{\theta'}(\theta',\phi')\\ F_{\phi'}(\theta',\phi')\end{pmatrix} \quad (5.1\text{-}11)$$

The angle ψ can be computed in numerous ways from equation (5.1-10), with one such way approach being

$$\psi=\arg\left(\hat{\theta}(\theta,\phi)^T R\hat{\theta}'(\theta',\phi')+j\,\hat{\phi}(\theta,\phi)^T R\hat{\theta}'(\theta',\phi')\right) \quad (5.1\text{-}12)$$

The dot products are readily computed using the Cartesian representation of the spherical unit vectors.
The general expressions for these unit vectors are given by

$$\hat{\theta} = \begin{pmatrix} \cos\theta\cos\phi \\ \cos\theta\sin\phi \\ -\sin\theta \end{pmatrix} \tag{5.1-13}$$

and

$$\hat{\phi} = \begin{pmatrix} -\sin\phi \\ +\cos\phi \\ 0 \end{pmatrix} \tag{5.1-14}$$

The angle ψ can be expressed as a function of mechanical orientation (α, β, γ) and spherical position (θ, ϕ), and is given by

$$\psi = \arg\begin{pmatrix} (\sin\gamma\cos\theta\sin(\phi-\alpha)+\cos\gamma(\cos\beta\sin\theta-\sin\beta\cos\theta\cos(\phi-\alpha)))+ \\ j(\sin\gamma\cos(\phi-\alpha)+\sin\beta\cos\gamma\sin(\phi-\alpha)) \end{pmatrix} \tag{5.1-15}$$

It can be shown that $\cos\psi$ and $\sin\psi$ can be expressed as:

$$\cos\psi = \frac{\cos\beta\cos\gamma\sin\theta-(\sin\beta\cos\gamma\cos(\phi-\alpha)-\sin\gamma\sin(\phi-\alpha))\cos\theta}{\sqrt{1-(\cos\beta\cos\gamma\cos\theta+(\sin\beta\cos\gamma\cos(\phi-\alpha)-\sin\gamma\sin(\phi-\alpha))\sin\theta)^2}} \tag{5.1-16}$$

$$\sin\psi = \frac{\sin\beta\cos\gamma\sin(\phi-\alpha)+\sin\gamma\cos(\phi-\alpha)}{\sqrt{1-(\cos\beta\cos\gamma\cos\theta+(\sin\beta\cos\gamma\cos(\phi-\alpha)-\sin\gamma\sin(\phi-\alpha))\sin\theta)^2}} \tag{5.1-17}$$

5.1.4 Transformation from an LCS to a GCS for downtilt angle only

In this clause equations are provided for the transformation from LCS to GCS assuming that the orientation of the LCS (with respect to the GCS) is such that the bearing angle α=0, the downtilt angle β is non-zero and the slant angle γ=0. In other words the y'-axis of the LCS is parallel to the y-axis of the GCS. Considering a BS antenna element the x-axis of the GCS is aligned with the pointing direction of the sector. Mechanical downtilt is modelled as a rotation of the LCS around the y-axis. For zero mechanical downtilt the LCS coincides with the GCS.

This transformation relates the spherical angles (θ, ϕ) in the global coordinate system to spherical angles (θ', ϕ') in the local (antenna-fixed) coordinate system and is defined as follows:

$$\theta' = \arccos(\cos\phi\sin\theta\sin\beta+\cos\theta\cos\beta), \tag{5.1-18}$$

$$\phi' = \arg(\cos\phi\sin\theta\cos\beta-\cos\theta\sin\beta+j\sin\phi\sin\theta), \tag{5.1-19}$$

where β is the mechanical tilt angle around the y-axis as defined in Figure 5.1.4.
Note that the equations (5.1-7), (5.1-8) reduce to equations (5.1-18), (5.1-19) if both α and γ are zero.

The antenna element pattern $A(\theta,\phi)$ in the GCS is related to the antenna element pattern $A'(\theta',\phi')$ in the LCS by the relation

$$A(\theta,\phi) = A'(\theta',\phi') \tag{5.1-20}$$

with θ' and ϕ' given by (5.1-18) and (5.1-19).

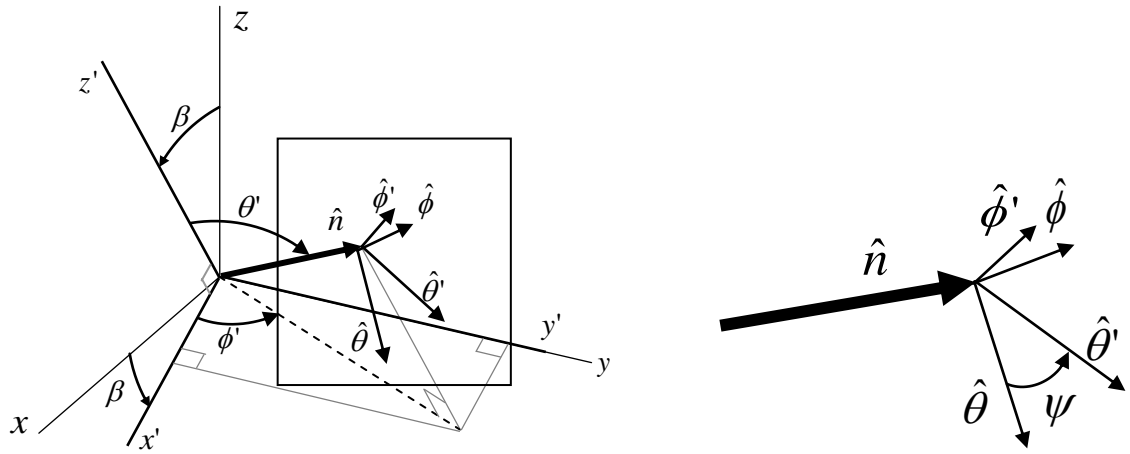

Figure 5.1.4: Definition of angles and unit vectors when the LCS has been rotated an angle β around the *y*-axis of the GCS

For a mechanical tilt angle β, the global coordinate system field components $F_\theta(\theta,\phi)$ and $F_\phi(\theta,\phi)$, are calculated from the field components $F_{\theta'}(\theta',\phi')$ and $F_{\phi'}(\theta',\phi')$ of the radiation pattern in the local (antenna-fixed) coordinate system as:

$$F_\theta(\theta,\phi) = F_{\theta'}(\theta',\phi')\cos\psi - F_{\phi'}(\theta',\phi')\sin\psi \tag{5.1-21}$$

$$F_\phi(\theta,\phi) = F_{\theta'}(\theta',\phi')\sin\psi + F_{\phi'}(\theta',\phi')\cos\psi \tag{5.1-22}$$

where θ' and ϕ' are defined as in (5.1-18) and (5.1-19), and ψ is defined as:

$$\psi = \arg\left(\sin\theta\cos\beta - \cos\phi\cos\theta\sin\beta + j\sin\phi\sin\beta\right). \tag{5.1-23}$$

Note that the equation (5.1-15) is reduced to equation (5.1-23) if both α and γ are zero.

As an example, in the horizontal cut, i.e., for $\theta = 90^\circ$, equations (5.1-18), (5.1-19) and (5.1-23) become

$$\theta' = \arccos(\cos\phi\sin\beta), \tag{5.1-24}$$

$$\phi' = \arg(\cos\phi\cos\beta + j\sin\phi), \tag{5.1-25}$$

$$\psi = \arg\left(\cos\beta + j\sin\phi\sin\beta\right). \tag{5.1-26}$$

6 Scenarios for UE specific elevation beamforming and FD-MIMO

Editor's note: Intended to identify the typical usage scenarios of UE-specific elevation beamforming and FD- MIMO

Scenario 3D-UMi: Urban Micro cell with high (outdoor/indoor) UE density

- Base Station (BS) is below surrounding buildings.

Scenario 3D-UMa: Urban Macro cell with high (outdoor/indoor) UE density

- BS is above surrounding buildings.

Scenario 3D-UMa-H: Urban Macro cell with one high-rise per sector and 300m ISD

- Density of high rise buildings is one per sector.

Scenario 3D-InH: Indoor Hotspot cell with high (indoor) UE density

- Base Station (BS) is mounted below the ceiling. The indoor test environment focuses on small cells and high user throughput inside of buildings. The key characteristics of this test environment are high user throughput and indoor coverage.

Table 6-1: 3D-UMi and 3D-UMa **scenario descriptions**

		Urban Micro cell with high UE density (3D-UMi)	**Urban Macro cell with high UE density (3D-UMa)**	**Urban Macro cell with one high-rise per sector and 300m ISD (3D-UMa-H)**
Clause-1				
Layout		Hexagonal grid, 19 micro sites,3 sectors per site	Hexagonal grid, 19 macro sites,3 sectors per site	Hexagonal grid, 19 macro sites,3 sectors per site
UE mobility (movement in horizontal plane)		3km/h	3km/h	3kmph
BS antenna height		10m	25m	25m
Total BS Tx Power		41/44 dBm for 10/20MHz	46/49 dBm for 10/20MHz	46/49 dBm for 10/20MHz
Carrier frequency		2 GHz	2 GHz	2 GHz
Min. UE-eNB 2D distance (note 1)		10m [other values are not precluded]	35m	35m
UE height (h_{UT}) in meters	general equation	$h_{UT}=3(n_{fl}-1)+1.5$	$h_{UT}=3(n_{fl}-1)+1.5$	$h_{UT}=3(n_{fl}-1)+1.5$
	n_{fl} for outdoor UEs	1	1	1
	n_{fl} for indoor UEs	n_{fl} ~ uniform(1,N_{fl}) where N_{fl} ~ uniform(4,8)	n_{fl} ~ uniform(1,N_{fl}) where N_{fl} ~ uniform(4,8)	n_{fl} ~ uniform(1,N_{fl})[3)]
Indoor UE fraction		80%	80%	80%
Clause-2 (note 2)				
UE distribution (in x-y plane)	Outdoor UEs	uniform in cell	uniform in cell	uniform in cell excluding high-rise building
	Indoor UEs	uniform in cell	uniform in cell	50% of indoor UEs within 25m radius of the high-rise building center, rest are outside the 25m radius.
ISD		200m	500m (not precluded option: 200m)	300m

NOTE 1: Refers to d_{2D} for outdoor UEs and $d_{2D\text{-}out}$ for indoor UEs as defined in Figure 3 and Figure 4 respectively.
NOTE 2: Assumptions in Clause-2 are for calibration purposes only in this SI.
Assumptions in Clause-2 are to be revisited for evaluating relative performance of proposed solutions in future SIs
NOTE 3: 50% of indoor UEs in a macro cell area are assumed to be inside a high-rise building and are associated with the same value of N_{fl}. The height of a high-rise given by N_{fl} ~ uniform(20,30). 50% of indoor UEs in a macro cell area are assumed to be outside the high-rise building and the associated N_{fl} for each UE ~ uniform(4,8).
NOTE 4: The channel modeling of 3D-UMa-H was discussed in RAN1#74, RAN1#74b, RAN1#75, RAN1#76. Example of modeling discussions can be found in [11-15] and references within.

Table 6-2: 3D-InH scenario description

Layout	Indoor floor plan given below
UE mobility (movement in horizontal plane)	3km/h
BS antenna height	3/6 m
Total BS Tx Power	24dBm
Carrier frequency	2, 4 GHz
Min. UE-eNB 2D distance	[3]m
UE height (h_{UT}) in meters	h_{UT}=1.5
UE distribution (in x-y plane)	Randomly and uniformly distributed over floorplan area
ISD	2-site: 60m 3-site: 40m 6-site Case A: 20m 6-site Case B: 40m in horizontal, 20m in vertical

The layouts of indoor hotspot are listed as below:

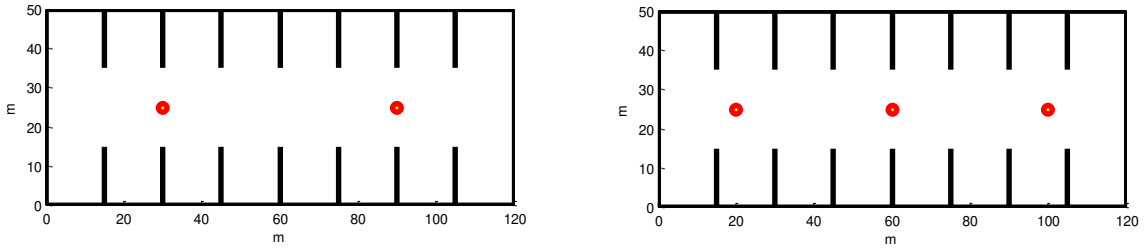

Figure 6-1: Indoor hotspot 2-site and 3-site deployment.

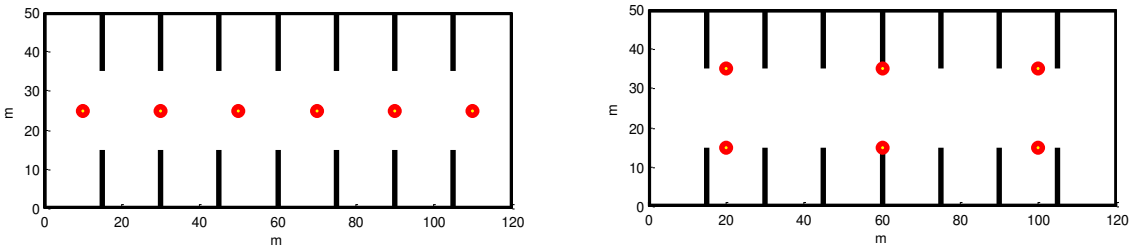

Case A **Case B**

Figure 6-2: Indoor hotspot 6-site deployment.

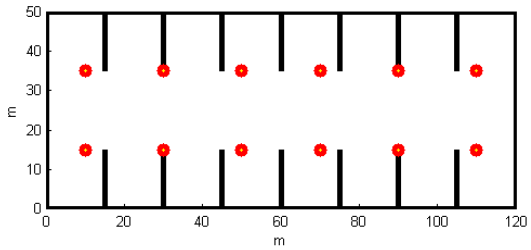

Figure 6-3: Indoor hotspot 12-site deployment.

Other typical usage scenaros of UE-specific elevation beamforming and FD- MIMO are noted below:

Heterogeneous Networks

- Channel models developed for Urban Micro cell with high UE density and Urban Macro cell with high UE density scenarios shall support heterogeneous deployment scenarios.
  - It is assumed that for heterogeneous deployment scenarios the macro BS height is at 25m and the lower-power node is at 10m height.
  - The carrier frequency(s) for a macro can be 2 or 3.5 GHz or both if multiple carriers are used.
    The carrier frequency(s) for a low power node can be 2 or 3.5 GHz or both if multiple carriers are used.
  - The transmission power of a low power node can be 30/33 dBm for 10/20 MHz.

Urban micro/macro homogeneous networks with high UE density (similar to 3D-UMi/3D-UMa) using higher than 2 GHz carrier frequency

- The carrier frequency can be 3.5 GHz.

7 3GPP evaluation methodology needed for Elevation Beamforming and FD-MIMO evaluation

Editor's note: The study will consider as a starting point the ITU channel model as described by the combination of A2.1.6 and Annex B in 36.814 [4] and determine the additions that are needed to properly model the elevation dimension of the channel to fit the elevation beamforming and FD-MIMO purposes]

The applicable range of the 3D channel model is at least for 2-3.5 GHz.

7.1 Antenna modelling

- 2D planar antenna array structure is the baseline, i.e., antenna elements are placed in the vertical and horizontal direction as below, where N is the number of columns, M is the number of antenna elements with the same polarization in each column. Antenna numbering below assumes observation of the antenna array from the front (with x-axis pointing towards broad-side and increasing y-coordinate for increasing column number).
- Antenna elements are uniformly spaced in the horizontal direction with a spacing of d_H and in the vertical direction with a spacing of d_V.

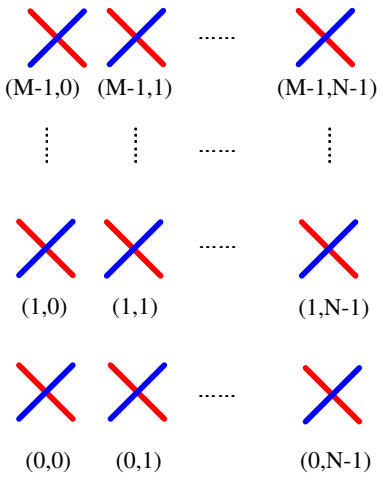

Figure 7.1-1: 2D planar antenna structure where each column is a cross-polarized array

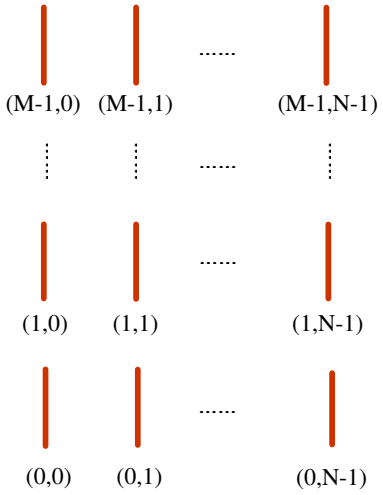

Figure 7.1-2: 2D planar antenna structure where each column is a uniform linear array

Table 7.1-1: Antenna modelling parameters

Parameter	Applicability	Values
Clause-1		
Number of horizontal antenna elements	cross-pol	2, 4, 8
	co-pol	1, 2, 4, 8
Polarization slant angle	cross-pol	+/- 45^0
	co-pol	0^0
Horizontal antenna element spacing d_H		0.5λ baseline (other values are not precluded)
Antenna element vertical radiation pattern (dB)		$A_{E,V}(\theta'') = -\min\left\{12\left(\frac{\theta''-90^\circ}{\theta_{3\text{dB}}}\right)^2, SLA_V\right\}, \theta_{3\text{dB}} = 65^\circ, SLA_V = 30\,\text{dB}$
Antenna element horizontal radiation pattern (dB)	3D-UMa, 3D-UMi, LPN deployments	$A_{E,H}(\phi'') = -\min\left\{12\left(\frac{\phi''}{\phi_{3\text{dB}}}\right)^2, A_m\right\}, \phi_{3\text{dB}} = 65^\circ, A_m = 30\,\text{dB}$
	3D-UMi, LPN deployments	Not precluded option: $A_{E,H}(\phi'') = 0$
Combining method for 3D antenna element pattern (dB)		$A''(\theta'',\phi'') = -\min\left\{-\left[A_{E,V}(\theta'') + A_{E,H}(\phi'')\right], A_m\right\}$
Maximum directional gain of an antenna element $G_{E,max}$		8 dBi
Clause-2 (note)		
Vertical antenna element spacing d_V		0.5λ, 0.8λ
Number of antenna elements with the same polarization in each column M		10 baseline, other values are not precluded
Complex weight for antenna element *m* in elevation		$w_m = \frac{1}{\sqrt{K}}\exp\left(-j\frac{2\pi}{\lambda}(m-1)d_V\cos\theta_{etilt}\right)$ where *m*=1,…,K. θ_{etilt} is the electrical vertical steering angle defined between 0^0 and 180^0 (90^0 represents perpendicular to the array). K = 1, M.
NOTE: Assumptions in clause-2 are for calibration of channel modelling		

7.1.1 Modelling polarized antennas

Model-1:

In case of polarized antenna elements assume ζ is the polarization slant angle where $\zeta = 0$ degrees corresponds to a purely vertically polarized antenna element and $\zeta = +/-45$ degrees correspond to a pair of cross polarized antenna elements. Then the antenna element field components in the elevation and azimuth polarization directions are given by

$$\begin{pmatrix} F_{\theta'}(\theta',\phi') \\ F_{\phi'}(\theta',\phi') \end{pmatrix} = \begin{pmatrix} +\cos\psi & -\sin\psi \\ +\sin\psi & +\cos\psi \end{pmatrix} \begin{pmatrix} F_{\theta''}(\theta'',\phi'') \\ F_{\phi''}(\theta'',\phi'') \end{pmatrix} \quad (7.1\text{-}1)$$

where $\cos\psi = \dfrac{\cos\zeta\sin\theta' + \sin\zeta\sin\phi'\cos\theta'}{\sqrt{1-(\cos\zeta\cos\theta' - \sin\zeta\sin\phi'\sin\theta')^2}}$, $\sin\psi = \dfrac{\sin\zeta\cos\phi'}{\sqrt{1-(\cos\zeta\cos\theta' - \sin\zeta\sin\phi'\sin\theta')^2}}$.

Note that the zenith and the azimuth field components $F_{\theta'}(\theta',\phi')$, $F_{\phi'}(\theta',\phi')$, $F_{\phi''}(\theta'',\phi'')$ and $F_{\phi''}(\theta'',\phi'')$ are defined in terms of the spherical basis vectors of an LCS as defined in clause 5.1.2. The difference between the single-primed and the double-primed components is that the single-primed field components account for the polarization slant and the double-primed field components do not. For a single polarized antenna (purely vertically polarized antenna) we can write $F_{\theta''}(\theta'',\phi'') = \sqrt{A''(\theta'',\phi'')}$ and $F_{\phi''}(\theta'',\phi'') = 0$ where $A''(\theta'',\phi'')$ is the 3D antenna element gain pattern as a function of azimuth angle ϕ'' and zenith angle θ'' in the LCS. The 3D antenna element gain pattern $A''(\theta'',\phi'')$ is defined in Table 7.1-1.

Model-2:

In case of polarized antennas, the polarization is modelled as angle-independent in both azimuth and elevation, in an LCS. For a linearly polarized antenna, the antenna element field pattern, in the vertical polarization and in the horizontal polarization, are given by

$$F_{\theta'}(\theta',\phi') = \sqrt{A'(\theta',\phi')}\cos(\zeta) \quad (7.1\text{-}2)$$

and

$$F_{\phi'}(\theta',\phi') = \sqrt{A'(\theta',\phi')}\sin(\zeta), \quad (7.1\text{-}3)$$

respectively, where ζ is the polarization slant angle and $A'(\theta',\phi')$ is the 3D antenna element gain pattern as a function of azimuth angle, ϕ' and elevation angle, θ' in the LCS. Note that $\zeta = 0$ degrees correspond to a purely vertically polarized antenna element. The vertical and horizontal field directions are defined in terms of the spherical basis vectors, $\hat{\theta}'$ and $\hat{\phi}'$ respectively in the LCS as defined in clause 5.1.2. Also $A'(\theta',\phi') = A''(\theta'',\phi'')$, $\theta' = \theta''$ and $\phi' = \phi''$ as defined in Table 7.1-1.

Typical antennas have polarization parallelity that is lower than the polarization parallelity of dipoles and, in addition, typical antennas have polarization parallelity close to zero in the main beam.
This observation is made from slide 5 in R1-140765 [6].

7.2 Pathloss, LOS probability and penetration modelling

7.2.1 Pathloss models

The pathloss models can be applied in the frequency range of 2 – 6 GHz and for different antenna heights. The pathloss models are summarized in Table 7.2-1 and the distance definitions are indicated in Figure 7.2-1 and Figure 7.2-2. Note that the distribution of the shadow fading is log-normal, and its standard deviation for each scenario is given in Table 7.2-1.

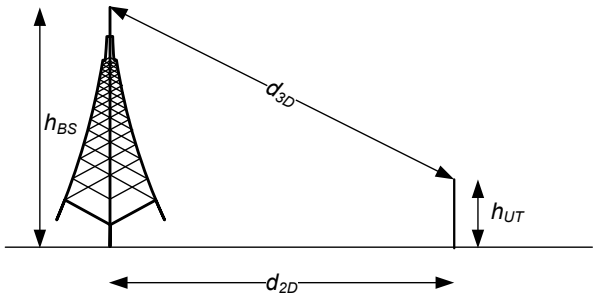

Figure7.2-1: Definition of d_{2D} and d_{3D} for outdoor UEs

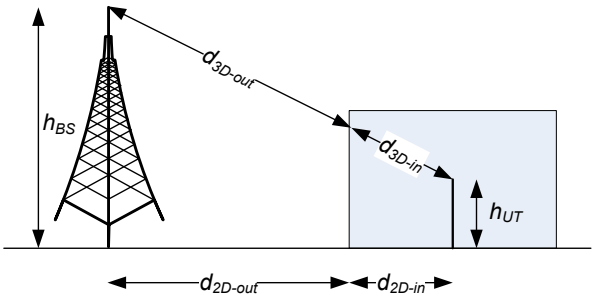

Figure 7.2-2: Definition of $d_{2D\text{-}out}$, $d_{2D\text{-}in}$ and $d_{3D\text{-}out}$, $d_{3D\text{-}in}$ for indoor UEs.

Note that

$$d_{\mathrm{3D-out}} + d_{\mathrm{3D-in}} = \sqrt{\left(d_{\mathrm{2D-out}} + d_{\mathrm{2D-in}}\right)^2 + \left(h_{\mathrm{BS}} - h_{\mathrm{UT}}\right)^2}$$

Table 7.2-1: Pathloss models

Scenario	LOS/NLOS	Pathloss [dB], f_c is in GHz and distance is in meters	Shadow fading std [dB][7)]	Applicability range, antenna height default values
3D-UMi	LOS	$PL = 22.0\log_{10}(d_{3D}) + 28.0 + 20\log_{10}(f_c)$ $PL = 40\log_{10}(d_{3D})+28.0+20\log_{10}(f_c) -9\log_{10}((d'_{BP})^2+(h_{BS} - h_{UT})^2)$	$\sigma_{SF} = 3$ $\sigma_{SF} = 3$	$10m < d_{2D} < d'_{BP}$ [1)] $d'_{BP} < d_{2D} < 5000m$ [1)] $h_{BS} = 10m$ [1)], $1.5m \leqq h_{UT} \leqq 22.5m$ [1)]
	NLOS	**For hexagonal cell layout:** $PL = max(PL_{3D\text{-}UMi\text{-}NLOS}, PL_{3D\text{-}UMi\text{-}LOS})$ $PL_{3D\text{-}UMi\text{-}NLOS} = 36.7\log_{10}(d_{3D}) + 22.7 + 26\log_{10}(f_c) - 0.3(h_{UT} - 1.5)$	$\sigma_{SF} = 4$	$10 m < d_{2D} < 2000m$ [2)] $h_{BS} = 10m$ $1.5m \leqq h_{UT} \leqq 22.5m$
3D-UMa	LOS	$PL = 22.0\log_{10}(d_{3D}) + 28.0 + 20\log_{10}(f_c)$ $PL = 40\log_{10}(d_{3D})+28.0+20\log_{10}(f_c) -9\log_{10}((d'_{BP})^2+(h_{BS} - h_{UT})^2)$	$\sigma_{SF} = 4$ $\sigma_{SF} = 4$	$10m < d_{2D} < d'_{BP}$ [4)] $d'_{BP} < d_{2D} < 5000m$ [4)] $h_{BS} = 25m$ [4)], $1.5m \leqq h_{UT} \leqq 22.5m$ [4)]
	NLOS	$PL = max(PL_{3D\text{-}UMa\text{-}NLOS}, PL_{3D\text{-}UMa\text{-}LOS})$ $PL_{3D\text{-}UMa\text{-}NLOS} = 161.04 - 7.1\log_{10}(W) + 7.5\log_{10}(h)$ $-(24.37 - 3.7(h/h_{BS})^2)\log_{10}(h_{BS})$ $+(43.42 - 3.1\log_{10}(h_{BS}))(\log_{10}(d_{3D}) - 3) + 20\log_{10}(f_c)$ $-(3.2(\log_{10}(17.625))^2 - 4.97) - 0.6(h_{UT} - 1.5)$	$\sigma_{SF} = 6$	$10 m < d_{2D} < 5\,000 m$ h = avg. building height, W = street width $h_{BS} = 25 m$, $1.5m \leqq h_{UT} \leqq 22.5m$, $W = 20m$, $h = 20 m$ The applicability ranges: $5 m < h < 50 m$ $5 m < W < 50 m$ $10 m < h_{BS} < 150 m$ $1.5 m \leqq h_{UT} \leqq 22.5 m$ Explanations: see [6)]
3D-RMa	LOS	$PL_1 = 20\log_{10}(40\pi d_{3D} f_c/3) + \min(0.03h^{1.72},10)\log_{10}(d_{3D})$ $-\min(0.044h^{1.72},14.77) + 0.002\log_{10}(h)d_{3D}$ $PL_2 = PL_1(d_{BP}) + 40\log_{10}(d_{3D}/d_{BP})$	$\sigma_{SF} = 4$ $\sigma_{SF} = 6$	$10 m < d_{2D} < d_{BP}$, [8)] $d_{BP} < d_{2D} < 10\,000 m$, $h_{BS} = 35 m$, $h_{UT} = 1.5 m$, $W = 20 m$, $h = 5 m$ h = avg. building height, W = street width The applicability ranges: $5 m < h < 50 m$ $5 m < W < 50 m$ $10 m < h_{BS} < 150 m$ $1 m < h_{UT} < 10 m$
	NLOS	$PL = 161.04 - 7.1\log_{10}(W) + 7.5\log_{10}(h)$ $-(24.37 - 3.7(h/h_{BS})^2)\log_{10}(h_{BS})$ $+(43.42 - 3.1\log_{10}(h_{BS}))(\log_{10}(d_{3D}) - 3) + 20\log_{10}(f_c)$ $-(3.2(\log_{10}(11.75\,h_{UT}))^2 - 4.97)$	$\sigma_{SF} = 8$	$10 m < d_{2D} < 5\,000 m$, $h_{BS} = 35 m$, $h_{UT} = 1.5 m$, $W = 20 m$, $h = 5 m$ h = avg. building height, W = street width The applicability ranges: $5 m < h < 50 m$ $5 m < W < 50 m$ $10 m < h_{BS} < 150 m$ $1 m < h_{UT} < 10 m$
3D-InH	LOS	$PL = 16.9\log_{10}(d_{3D}) + 32.8 + 20\log_{10}(f_c)$	$\sigma_{SF} = 3$	$3 m < d_{2D} < 150 m$ $h_{BS} = 3\text{-}6 m$ $h_{UT} = 1\text{-}2.5 m$
	NLOS	$PL = 43.3\log_{10}(d_{3D}) + 11.5 + 20\log_{10}(f_c)$	$\sigma_{SF} = 4$	$10 m < d_{2D} < 150 m$ $h_{BS} = 3\text{-}6 m$ $h_{UT} = 1\text{-}2.5 m$

NOTE 1: Break point distance $d'_{BP} = 4\ h'_{BS}\ h'_{UT}\ f_c/c$, where f_c is the centre frequency in Hz, $c = 3.0\times10^8$ m/s is the propagation velocity in free space, and h'_{BS} and h'_{UT} are the effective antenna heights at the BS and the UT, respectively. In 3D-UMi scenario the effective antenna heights h'_{BS} and h'_{UT} are computed as follows: $h'_{BS} = h_{BS} - 1.0$ m, $h'_{UT} = h_{UT} - 1.0$ m, where h_{BS} and h_{UT} are the actual antenna heights, and the effective environment height is assumed to be equal to 1.0 m.

NOTE 2: $PL_{3D\text{-}UMi\text{-}LOS}$ = Pathloss of 3D-UMi LOS outdoor scenario.

NOTE 4: Break point distance $d'_{BP} = 4\ h'_{BS}\ h'_{UT}\ f_c/c$, where f_c is the centre frequency in Hz, $c = 3.0\times10^8$ m/s is the propagation velocity in free space, and h'_{BS} and h'_{UT} are the effective antenna heights at the BS and the UT, respectively. In 3D-UMa scenario the effective antenna heights h'_{BS} and h'_{UT} are computed as follows: $h'_{BS} = h_{BS} - h_E$, $h'_{UT} = h_{UT} - h_E$, where h_{BS} and h_{UT} are the actual antenna heights, and the effective environment height h_E is a function of the link between a BS and a UT. In the event that the link is determined to be LOS, h_E=1m with a probability equal to $1/(1+C(d_{2D}, h_{UT}))$ and chosen from a discrete uniform distribution uniform(12,15,…,(h_{UT}-1.5)) otherwise. The function $C(d_{2D}, h_{UT})$ is defined in Table 7.2-2. Note that h_E depends on d_{2D} and h_{UT} and thus needs to be independently determined for every link between BS sites and UTs. A BS site may be a single BS or multiple co-located BSs.

NOTE 6: $PL_{3D\text{-}UMa\text{-}LOS}$ = Pathloss of 3D-UMa LOS outdoor scenario.

NOTE 7: The shadow fading values are reused from [4] for simplicity.

NOTE 8: Break point distance $d_{BP} = 2\pi\ h_{BS}\ h_{UT}\ f_c/c$, where f_c is the centre frequency in Hz, $c = 3.0\times10^8$ m/s is the propagation velocity in free space, and h_{BS} and h_{UT} are the antenna heights at the BS and the UT, respectively.

7.2.2 LOS probability

The Line-Of-Sight (LOS) probabilities are given in the following table.

Table 7.2-2: LOS probabilities

Scenario	LOS probability (distance is in meters)
3D-UMi	$\Pr_{\text{LOS}} = \begin{cases} 1 & ,d_{\text{2D-out}} \le 18\text{m} \\ \frac{18}{d_{\text{2D-out}}} + \exp\left(-\frac{d_{\text{2D-out}}}{36}\right)\left(1-\frac{18}{d_{\text{2D-out}}}\right) & ,18\text{m} < d_{\text{2D-out}} \end{cases}$
3D-UMa	$\Pr_{\text{LOS}} = \begin{cases} 1 & ,d_{\text{2D-out}} \le 18\text{m} \\ \left[\frac{18}{d_{\text{2D-out}}} + \exp\left(-\frac{d_{\text{2D-out}}}{63}\right)\left(1-\frac{18}{d_{\text{2D-out}}}\right)\right]\left(1 + C'(h_{\text{UT}})\frac{5}{4}\left(\frac{d_{\text{2D-out}}}{100}\right)^3 \exp\left(-\frac{d_{\text{2D-out}}}{150}\right)\right) & ,18\text{m} < d_{\text{2D-out}} \end{cases}$ where $C'(h_{\text{UT}}) = \begin{cases} 0 & ,h_{\text{UT}} \le 13\text{m} \\ \left(\frac{h_{\text{UT}}-13}{10}\right)^{1.5} & ,13\text{m} < h_{\text{UT}} \le 23\text{m} \end{cases}$
3D-RMa	$\Pr_{\text{LOS}} = \begin{cases} 1 & ,d_{\text{2D-out}} \le 10\text{m} \\ \exp\left(-\frac{d_{\text{2D-out}}-10}{1000}\right) & ,10\text{m} < d_{\text{2D-out}} \end{cases}$
3D-InH	For 2 sites, 3 sites, and 6 sites Case A $\Pr_{\text{LOS}} = \begin{cases} 1 & ,d_{\text{2D-in}} \le 18\text{m} \\ \exp\left(-\frac{d_{\text{2D-in}}-18}{27}\right) & ,18\text{m} < d_{\text{2D-in}} < 37\text{m} \\ 0.5 & ,37\text{m} \le d_{\text{2D-in}} \end{cases}$ For 6 sites Case B and 12 sites $\Pr_{\text{LOS}} = \begin{cases} 1 & ,d_{\text{2D-in}} \le 5\text{m} \\ \exp\left(-\frac{d_{\text{2D-in}}-5}{70.8}\right) & ,5\text{m} < d_{\text{2D-in}} \le 49\text{m} \\ \exp\left(-\frac{d_{\text{2D-in}}-49}{211.7}\right)\cdot 0.54 & ,49\text{m} < d_{\text{2D-in}} \end{cases}$

7.2.3 O2I penetration loss

3D-UMi O2I	$PL = PL_b + PL_{tw} + PL_{in}$ **For hexagonal cell layout:** $PL_b = PL_{3D\text{-}UMi}(d_{3D\text{-}out} + d_{3D\text{-}in})$ $PL_{tw} = 20$ $PL_{in} = 0.5d_{2D\text{-}in}$	σ_{SF} =7	10m < $d_{2D\text{-}out} + d_{2D\text{-}in}$ < 1000m 0m < $d_{2D\text{-}in}$ < 25m h_{BS} = 10m, h_{UT}=3(n_{fl} – 1) + 1.5, n_{fl} = 1, 2, 3, 4, 5, 6, 7, 8. Explanations: see [3)]
NOTE 3: PL_b = basic path-loss, $PL_{3D\text{-}UMi}$ = Loss of 3D-UMi outdoor scenario, PL_{tw} = Loss through wall, PL_{in} = Loss inside, $d_{2D\text{-}in}$ is assumed uniformly distributed between 0 and 25 m.			

3D-UMa O2I	$PL = PL_b + PL_{tw} + PL_{in}$ **For hexagonal cell layout:** $PL_b = PL_{3D\text{-}UMa}(d_{3D\text{-}out} + d_{3D\text{-}in})$ $PL_{tw} = 20$ $PL_{in} = 0.5d_{2D\text{-}in}$	σ_{SF} =7	10m < $d_{2D\text{-}out} + d_{2D\text{-}in}$ < 1000m 0m < $d_{2D\text{-}in}$ < 25m h_{BS} = 25m, h_{UT}=3(n_{fl} – 1) + 1.5, n_{fl} = 1, 2, 3, 4, 5, 6, 7, 8. Explanations: see [5)]
NOTE 5: PL_b = basic path-loss, $PL_{3D\text{-}UMa}$ = Loss of 3D-UMa outdoor scenario, PL_{tw} = Loss through wall, PL_{in} = Loss inside, $d_{2D\text{-}in}$ is assumed uniformly distributed between 0 and 25 m.			

7.2.4 Autocorrelation of shadow fading

The long-term (log-normal) fading in the logarithmic scale around the mean path loss PL (dB) is characterized by a Gaussian distribution with zero mean and standard deviation. Due to the slow fading process versus distance Δx (Δx is in the horizontal plane), adjacent fading values are correlated. Its normalized autocorrelation function $R(\Delta x)$ can be described with sufficient accuracy by the exponential function ITU-R Rec. P.1816 [5]

$$R(\Delta x) = \mathrm{e}^{-\frac{|\Delta x|}{d_{cor}}} \tag{7.2-1}$$

with the correlation length d_{cor} being dependent on the environment, see the correlation parameters for shadowing and other large scale parameters in Table 7.3-6 (Channel model parameters for 3D-UMi and 3D-UMa), Table 7.3-6a (Channel model parameters for 3D-InH) and Table 7.3-6b (Channel model parameters for 3D-RMa).

7.3 Fast fading model

The radio channels are created using the parameters listed in Table 7.3-6. The channel realizations are obtained by a step-wise procedure illustrated in Figure 7.3-1 and described below. It has to be noted that the geometric description covers arrival angles from the last bounce scatterers and respectively departure angles to the first scatterers interacted from the transmitting side. The propagation between the first and the last interaction is not defined. Thus, this approach can model also multiple interactions with the scattering media. This indicates also that e.g., the delay of a multipath component cannot be determined by the geometry. In the following steps, downlink is assumed. For uplink, arrival and departure parameters have to be swapped. Note that channel coefficient generation (steps 4 to 11) for LOS O2I case follow the same method as the NLOS case.

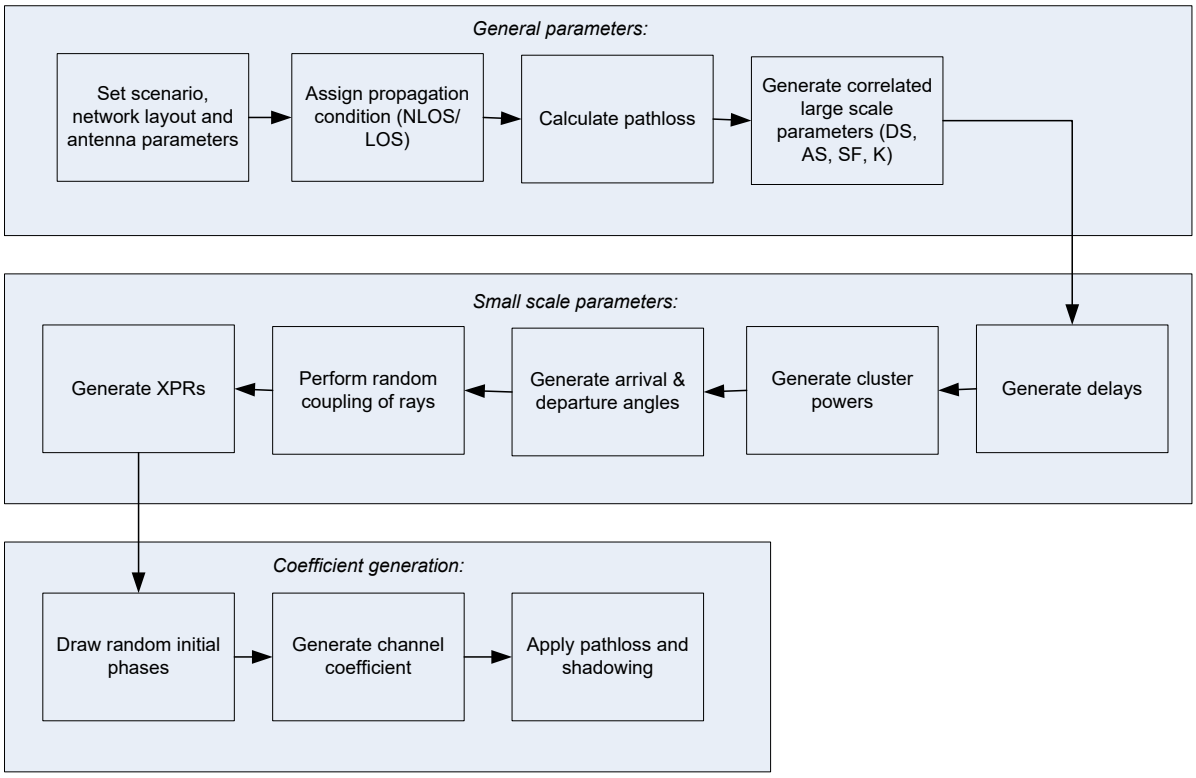

Figure 7.3-1: Channel coefficient generation procedure

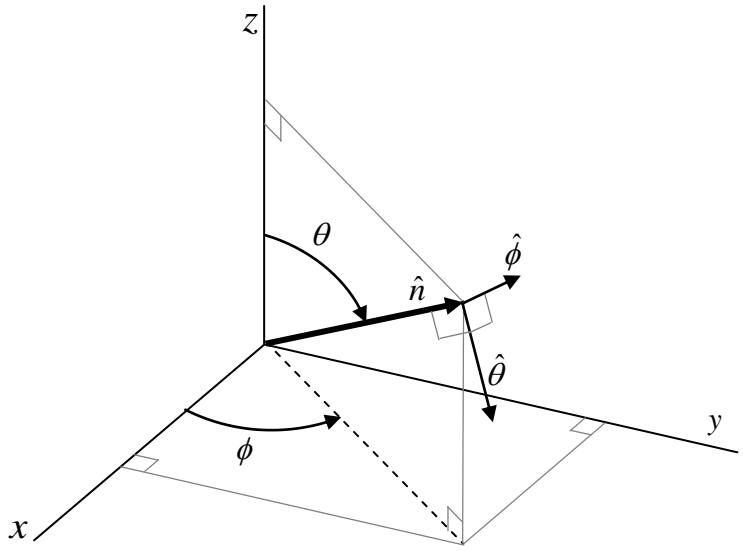

Figure 7.3-2: Definition of a global coordinate system showing the zenith angle θ and the azimuth angle ϕ. θ=0^0 points to zenith and θ=+90^0 points to the horizon.
The spherical basis vectors $\hat{\theta}$ and $\hat{\phi}$ shown above are defined based on the direction of propagation $\hat{n}$.

Table 7.3-1: Notations in the global coordinate system (GCS)

Parameter	Notation	Comments
LOS AOD	$\phi_{LOS,AOD}$	defined by ϕ
LOS AOA	$\phi_{LOS,AOA}$	defined by ϕ
LOS ZOD	$\theta_{LOS,ZOD}$	defined by θ
LOS ZOA	$\theta_{LOS,ZOA}$	defined by θ
AOA for cluster *n*	$\phi_{n,AOA}$	defined by ϕ
AOD for cluster *n*	$\phi_{n,AOD}$	defined by ϕ
AOA for ray *m* in cluster *n*	$\phi_{n,m,AOA}$	defined by ϕ
AOD for ray *m* in cluster *n*	$\phi_{n,m,AOD}$	defined by ϕ
ZOA for cluster *n*	$\theta_{n,ZOA}$	defined by θ
ZOD for cluster *n*	$\theta_{n,ZOD}$	defined by θ
ZOA for ray *m* in cluster *n*	$\theta_{n,m,ZOA}$	defined by θ
ZOD for ray *m* in cluster *n*	$\theta_{n,m,ZOD}$	defined by θ
Receive antenna element *u* field pattern in the direction of the spherical basis vector $\hat{\theta}$	$F_{rx,u,\theta}$	
Receive antenna element *u* field pattern in the direction of the spherical basis vector $\hat{\phi}$	$F_{rx,u,\phi}$	
Transmit antenna element *s* field pattern in the direction of the spherical basis vector $\hat{\theta}$	$F_{tx,s,\theta}$	
Transmit antenna element *s* field pattern in the direction of the spherical basis vector $\hat{\phi}$	$F_{rx,s,\phi}$	

General parameters:

Step 1: Set environment, network layout, and antenna array parameters

a) Choose one of the scenarios (3D-UMa, 3D-UMi, 3D-Rma, 3D-InH). Choose a global coordinate system and define zenith angle θ, azimuth angle ϕ, and spherical basis vectors $\hat{\theta}$, $\hat{\phi}$ as shown in Figure 7.3-2.

b) Give number of BS and UT

c) Give 3D locations of BS and UT, and LOS AOD ($\phi_{LOS,AOD}$), LOS ZOD ($\theta_{LOS,ZOD}$), LOS AOA ($\phi_{LOS,AOA}$), LOS ZOA ($\theta_{LOS,ZOA}$) of each BS and UT in the global coordinate system

d) Give BS and UT antenna field patterns F_{rx} and F_{tx} in the global coordinate system and array geometries

e) Give BS and UT array orientations with respect to the global coordinate system. BS array orientation is defined by three angles $\Omega_{BS,\alpha}$ (BS bearing angle), $\Omega_{BS,\beta}$ (BS downtilt angle) and $\Omega_{BS,\gamma}$ (BS slant angle). UT array orientation is defined by three angles $\Omega_{UT,\alpha}$ (UT bearing angle), $\Omega_{UT,\beta}$ (UT downtilt angle) and $\Omega_{UT,\gamma}$ (UT slant angle).

f) Give speed and direction of motion of UT in the global coordinate system

g) Give system centre frequency

Large scale parameters:

Step 2: Assign propagation condition (LOS/NLOS) according to Table 7.2-2.

Step 3: Calculate pathloss with formulas of Table 7.2-1 for each BS-UT link to be modelled.

Step 4: Generate large scale parameters e.g. delay spread (DS), angular spreads (ASA, ASD, ZSA, ZSD), Ricean K factor (K) and shadow fading (SF) taking into account cross correlation according to Table 7.3-6 and using the procedure described in subclause 3.3.1 of [16] with the square root matrix $\sqrt{C_{MxM}(0)}$ being generated using the Cholesky decomposition and the following order of the large scale parameter vector: $\mathbf{s}_M = [s_{SF}, s_K, s_{DS}, s_{ASD}, s_{ASA}, s_{ZSD}, s_{ZSA}]^T$. Limit random RMS azimuth arrival and azimuth departure spread values to 104 degrees, i.e., ASA = min(ASA,

104°), ASD = min(ASD, 104°). Limit random RMS zenith arrival and zenith departure spread values to 52 degrees, i.e., ZSA = min(ZSA, 52°), ZSD = min(ZSD, 52°).

Small scale parameters:

Step 5: Generate cluster delays τ_n.

Delays are drawn randomly from the delay distribution defined in Table 7.3-6. With exponential delay distribution calculate

$$\tau_n' = -r_\tau \mathrm{DS} \ln\left(X_n\right), \tag{7.3-1}$$

Where r_τ is the delay distribution proportionality factor, X_n ~ uniform(0,1), and cluster index $n = 1,\ldots,N$. With uniform delay distribution the delay values τ_n' are drawn from the corresponding range. Normalise the delays by subtracting the minimum delay and sort the normalised delays to ascending order:

$$\tau_n = \mathrm{sort}\left(\tau_n' - \min\left(\tau_n'\right)\right). \tag{7.3-2}$$

In the case of LOS condition, additional scaling of delays is required to compensate for the effect of LOS peak addition to the delay spread. The heuristically determined Ricean K-factor dependent scaling constant is

$$C_\tau = 0.7705 - 0.0433K + 0.0002K^2 + 0.000017K^3, \tag{7.3-3}$$

where K [dB] is the Ricean K-factor as generated in Step 4. The scaled delays

$$\tau_n^{LOS} = \tau_n / C_\tau, \tag{7.3-4}$$

are **not** to be used in cluster power generation.

Step 6: Generate cluster powers P_n.

Cluster powers are calculated assuming a single slope exponential power delay profile. Power assignment depends on the delay distribution defined in Table 7.3-1. With exponential delay distribution the cluster powers are determined by

$$P_n' = \exp\left(-\tau_n \frac{r_\tau - 1}{r_\tau \mathrm{DS}}\right) \cdot 10^{\frac{-Z_n}{10}} \tag{7.3-5}$$

where $Z_n \sim N\left(0, \zeta^2\right)$ is the per cluster shadowing term in [dB]. Normalize the cluster powers so that the sum of all cluster powers is equal to one, i.e.,

$$P_n = \frac{P_n'}{\sum_{n=1}^{N} P_n'} \tag{7.3-6}$$

In the case of LoS condition an additional specular component is added to the first cluster. Power of the single LoS ray is:

$$P_{1,LOS} = \frac{K_R}{K_R + 1} \tag{7.3-7}$$

and the cluster powers are not as in equation (7.3-6), but:

$$P_n = \frac{1}{K_R + 1} \frac{P_n'}{\sum_{n=1}^{N} P_n'} + \delta(n-1) P_{1,LOS} \tag{7.3-8}$$

where δ(.) is Dirac's delta function and K_R is the Ricean *K*-factor as generated in Step 4 converted to linear scale. These power values are used *only* in equations (7.3-9) and (7.3-14), but *not* in equation (7.3-22).

Assign the power of each ray within a cluster as P_n / M, where M is the number of rays per cluster.

Remove clusters with less than -25 dB power compared to the maximum cluster power. The scaling factors need not be changed after cluster elimination.

Step 7: Generate arrival angles and departure angles for both azimuth and elevation.

The composite PAS in azimuth of all clusters is modelled as wrapped Gaussian, except for the indoor hotspot scenario (3D-InH) which is modelled by a wrapped Laplacian distribution. For the other scenarios the AOAs are determined by applying the inverse Gaussian function (7.3-9) with input parameters P_n and RMS angle spread ASA

$$\phi'_{n,AOA} = \frac{2(\mathrm{ASA}/1.4)\sqrt{-\ln\left(P_n/\max\left(P_n\right)\right)}}{C_\phi} \tag{7.3-9}$$

while the following inverse Laplacian function is used for the 3D-InH scenario

$$\phi'_{n,AOA} = \frac{-\mathrm{ASA}\ln\left(P_n/\max\left(P_n\right)\right)}{C_\phi}. \tag{7.3-9a}$$

In case of 3D-UMa and 3D-UMi C_ϕ is given by

$$C_\phi = \begin{cases} C_\phi^{\mathrm{NLOS}} \cdot \left(1.1035 - 0.028K - 0.002K^2 + 0.0001K^3\right) & \text{, for LOS} \\ C_\phi^{\mathrm{NLOS}} & \text{, for NLOS} \end{cases}, \tag{7.3-10}$$

while in case of 3D-InH it is given by

$$C_\phi = \begin{cases} C_\phi^{\mathrm{NLOS}} \cdot \left(0.9275 + 0.0439K - 0.0071K^2 + 0.0002K^3\right) & \text{, for LOS} \\ C_\phi^{\mathrm{NLOS}} & \text{, for NLOS} \end{cases}, \tag{7.3-10a}$$

where C_ϕ^{NLOS} is defined as a scaling factor related to the total number of clusters *N* and is given in the following table.

Table 7.3-2: Scaling factors for AOA, AOD generation

scenario	3D-UMa, 3D-UMi, 3D-RMa											3D-InH	
N	4	5	8	10	11	12	14	15	16	19	20	15	19
C_ϕ^{NLOS}	0.779	0.860	1.018	1.090	1.123	1.146	1.190	1.211	1.226	1.273	1.289	1.434	1.501

In the LOS case, C_ϕ is dependent also on the Ricean K-factor K in [dB], as generated in Step 4. Additional scaling of the angles is required to compensate for the effect of LOS peak addition to the angle spread.

Assign positive or negative sign to the angles by multiplying with a random variable X_n with uniform distribution to the discrete set of {1,–1}, and add component $Y_n \sim N\left(0,\left(\mathrm{ASA}/7\right)^2\right)$ to introduce random variation

$$\phi_{n,AOA} = X_n\phi'_{n,AOA} + Y_n + \phi_{LOS,AOA}, \tag{7.3-11}$$

where $\phi_{LOS,AOA}$ is the LOS direction defined in the network layout description, see Step1c.

In the LOS case, substitute (7.3-11) by (7.3-12) to enforce the first cluster to the LOS direction $\phi_{LOS,AOA}$

$$\phi_{n,AOA} = \left(X_n\phi'_{n,AOA} + Y_n\right) - \left(X_1\phi'_{1,AOA} + Y_1 - \phi_{LOS,AOA}\right). \tag{7.3-12}$$

Finally add offset angles α_m from Table 7.3-3 to the cluster angles

$$\phi_{n,m,AOA} = \phi_{n,AOA} + c_{\text{ASA}}\alpha_m, \tag{7.3-13}$$

where c_{ASA} is the cluster-wise rms azimuth spread of arrival angles (cluster ASA) in Table 7.3-6 and Table 7.3-6a.

Table 7.3-3: Ray offset angles within a cluster, given for 1 rms angle spread

Ray number *m*	Basis vector of offset angles α_m
1,2	± 0.0447
3,4	± 0.1413
5,6	± 0.2492
7,8	± 0.3715
9,10	± 0.5129
11,12	± 0.6797
13,14	± 0.8844
15,16	± 1.1481
17,18	± 1.5195
19,20	± 2.1551

The generation of AOD ($\phi_{n,m,\text{AOD}}$) follows a procedure similar to AOA as described above.

The generation of ZOA assumes that the composite PAS in the zenith dimension of all clusters is Laplacian. The ZOAs are determined by applying the inverse Laplacian function

$$\theta'_{n,ZOA} = \frac{-\text{ZSA}\ln\left(P_n/\max\left(P_n\right)\right)}{C_\theta} \tag{7.3-14}$$

with input parameters P_n, RMS angle spread ZSA, while

C_θ is defined as

$$C_\theta = \begin{cases} C_\theta^{\text{NLOS}} \cdot \left(1.35 + 0.0202K - 0.0077K^2 + 0.0002K^3\right) & \text{, for LOS} \\ C_\theta^{\text{NLOS}} & \text{, for NLOS} \end{cases} \tag{7.3-15}$$

where C_θ^{NLOS} is a scaling factor related to the total number of clusters and is given in the following table.

Table 7.3-4: Scaling factors for ZOA, ZOD generation

scenario	3D-UMa, 3D-UMi, 3D-InH, 3D-RMa					
N	**10**	**11**	**12**	**15**	**19**	**20**
C_θ^{NLOS}	0.9854	1.013	1.04	1.1088	1.1764	1.1918

In the LOS case, C_θ is dependent also on the Ricean K-factor K in [dB], as generated in Step 4. Additional scaling of the angles is required to compensate for the effect of LOS peak addition to the angle spread.

Assign positive or negative sign to the angles by multiplying with a random variable X_n with uniform distribution to the discrete set of {1,–1}, and add component $Y_n \sim N\left(0,\left(\text{ZSA}/7\right)^2\right)$ to introduce random variation

$$\theta_{n,ZOA} = X_n\theta'_{n,ZOA} + Y_n + \bar{\theta}_{ZOA}, \tag{7.3-16}$$

where $\bar{\theta}_{ZOA} = 90^0$ if the UT is located indoors and $\bar{\theta}_{ZOA} = \theta_{LOS,ZOA}$ if the UT is located outdoors. The LOS direction is defined in the network layout description, see Step1c.

In the LOS case, substitute (7.3-16) by (7.3-17) to enforce the first cluster to the LOS direction $\theta_{LOS,ZOA}$

$$\theta_{n,ZOA} = \left(X_n\theta'_{n,ZOA} + Y_n\right) - \left(X_1\theta'_{1,ZOA} + Y_1 - \theta_{LOS,ZOA}\right). \quad (7.3\text{-}17)$$

Finally add offset angles α_m from Table 7.3-3 to the cluster angles

$$\theta_{n,m,ZOA} = \theta_{n,ZOA} + c_{\text{ZSA}}\alpha_m, \quad (7.3\text{-}18)$$

where c_{ZSA} is the cluster-wise rms zenith spread of arrival (cluster ZSA) in Tables 7.3-6 and 7.3-6a. Assuming that $\theta_{n,m,ZOA}$ is wrapped within $[0,360^0]$, if $\theta_{n,m,ZOA} \in [180^0, 360^0]$, then $\theta_{n,m,ZOA}$ is set to $(360^0 - \theta_{n,m,ZOA})$.

The generation of ZOD follows the same procedure as ZOA described above except equation (7.3-16) is replaced by

$$\theta_{n,ZOD} = X_n\theta'_{n,ZOD} + Y_n + \theta_{LOS,ZOD} + \mu_{offset,ZOD}, \quad (7.3\text{-}19)$$

where variable X_n is with uniform distribution to the discrete set of {1,–1}, $Y_n \sim N\left(0, (\text{ZSD}/7)^2\right)$, $\mu_{offset,ZOD}$ is given in Tables 7.3-7, 7.3-8 and equation (7.3-18) is replaced by

$$\theta_{n,m,ZOD} = \theta_{n,ZOD} + (3/8)(10^{\mu_{\text{lgZSD}}})\alpha_m \quad (7.3\text{-}20)$$

where μ_{lgZSD} is the mean of the ZSD log-normal distribution.

In the LOS case, the generation of ZOD follows the same procedure as ZOA described above using equation (7.3-17).

Step 8: Coupling of rays within a cluster for both azimuth and elevation

Couple randomly AOD angles $\phi_{n,m,AOD}$ to AOA angles $\phi_{n,m,AOA}$ within a cluster *n*, or within a sub-cluster in the case of two strongest clusters (see Step 11 and Table 7.3-3). Couple randomly ZOD angles $\theta_{n,m,ZOD}$ with ZOA angles $\theta_{n,m,ZOA}$ using the same procedure. Couple randomly AOD angles $\phi_{n,m,AOD}$ with ZOD angles $\theta_{n,m,ZOD}$ within a cluster *n* or within a sub-cluster in the case of two strongest clusters.

Step 9: Generate XPRs

Generate the cross polarization power ratios (XPR) κ for each ray *m* of each cluster *n*. XPR is log-Normal distributed. Draw XPR values as

$$\kappa_{n,m} = 10^{X_{n,m}/10}, \quad (7.3\text{-}21)$$

where $X_{n,m} \sim N(\mu_{\text{XPR}}, \sigma^2_{\text{XPR}})$ is Gaussian distributed with σ_{XPR} and μ_{XPR} from Tables 7.3-6 and 7.3-6a. Note: $X_{n,m}$ is independently drawn for each ray and each cluster.

Coefficient generation:

Step 10: Draw initial random phases

Draw random initial phase $\left\{\Phi_{n,m}^{\theta\theta}, \Phi_{n,m}^{\theta\phi}, \Phi_{n,m}^{\phi\theta}, \Phi_{n,m}^{\phi\phi}\right\}$ for each ray *m* of each cluster *n* and for four different polarisation combinations ($\theta\theta$, $\theta\phi$, $\phi\theta$, $\phi\phi$). The distribution for initial phases is uniform within ($-\pi,\pi$).

In the LOS case, draw also a random initial phase Φ_{LOS} for both $\theta\theta$ and $\phi\phi$ polarisations.

Step 11: Generate channel coefficients for each cluster n and each receiver and transmitter element pair u, s.

For the N – 2 weakest clusters, say $n = 3, 4, \ldots, N$, the channel coefficients are given by:

$$H_{u,s,n}(t) = \sqrt{P_n/M}\sum_{m=1}^{M}\begin{bmatrix} F_{rx,u,\theta}\left(\theta_{n,m,ZOA},\phi_{n,m,AOA}\right) \\ F_{rx,u,\phi}\left(\theta_{n,m,ZOA},\phi_{n,m,AOA}\right)\end{bmatrix}^T \begin{bmatrix} \exp\left(j\Phi_{n,m}^{\theta\theta}\right) & \sqrt{\kappa_{n,m}^{-1}}\exp\left(j\Phi_{n,m}^{\theta\phi}\right) \\ \sqrt{\kappa_{n,m}^{-1}}\exp\left(j\Phi_{n,m}^{\phi\theta}\right) & \exp\left(j\Phi_{n,m}^{\phi\phi}\right)\end{bmatrix} \begin{bmatrix} F_{tx,s,\theta}\left(\theta_{n,m,ZOD},\phi_{n,m,AOD}\right) \\ F_{tx,s,\phi}\left(\theta_{n,m,ZOD},\phi_{n,m,AOD}\right)\end{bmatrix} \exp\left(j2\pi\lambda_0^{-1}\left(\hat{r}_{rx,n,m}^T.\bar{d}_{rx,u}\right)\right)\exp\left(j2\pi\lambda_0^{-1}\left(\hat{r}_{tx,n,m}^T.\bar{d}_{tx,s}\right)\right)\exp\left(j2\pi v_{n,m}t\right) \quad (7.3\text{-}22)$$

where $F_{rx,u,\theta}$ and $F_{rx,u,\phi}$ are the receive antenna element u field patterns in the direction of the spherical basis vectors, $\hat{\theta}$ and $\hat{\phi}$ respectively, $F_{tx,s,\theta}$ and $F_{tx,s,\phi}$ are the transmit antenna element s field patterns in the direction of the spherical basis vectors, $\hat{\theta}$ and $\hat{\phi}$ respectively. $\hat{r}_{rx,n,m}$ is the spherical unit vector with azimuth arrival angle $\phi_{n,m,AOA}$ and elevation arrival angle $\theta_{n,m,ZOA}$, given by

$$\hat{r}_{rx,n,m} = \begin{bmatrix} \sin\theta_{n,m,ZOA}\cos\phi_{n,m,AOA} \\ \sin\theta_{n,m,ZOA}\sin\phi_{n,m,AOA} \\ \cos\theta_{n,m,ZOA}\end{bmatrix}, \quad (7.3\text{-}23)$$

where n denotes a cluster and m denotes a ray within cluster n. $\hat{r}_{tx,n,m}$ is the spherical unit vector with azimuth departure angle $\phi_{n,m,AOD}$ and elevation departure angle $\theta_{n,m,ZOD}$, given by

$$\hat{r}_{tx,n,m} = \begin{bmatrix} \sin\theta_{n,m,ZOD}\cos\phi_{n,m,AOD} \\ \sin\theta_{n,m,ZOD}\sin\phi_{n,m,AOD} \\ \cos\theta_{n,m,ZOD}\end{bmatrix}, \quad (7.3\text{-}24)$$

where n denotes a cluster and m denotes a ray within cluster n. Also, $\bar{d}_{rx,u}$ is the location vector of receive antenna element u and $\bar{d}_{tx,s}$ is the location vector of transmit antenna element s, $\kappa_{n,m}$ is the cross polarisation power ratio in linear scale, and λ_0 is the wavelength of the carrier frequency. If polarisation is not considered, the 2x2 polarisation matrix can be replaced by the scalar $\exp\left(j\Phi_{n,m}\right)$ and only vertically polarised field patterns are applied.

The Doppler frequency component $v_{n,m}$ is calculated from the arrival angles (AOA, ZOA), UT velocity vector $\bar{v}$ with speed v, travel azimuth angle ϕ_v, elevation angle θ_v and is given by

$$v_{n,m} = \frac{\hat{r}_{rx,n,m}^T.\bar{v}}{\lambda_0}, \text{where } \bar{v} = v.\left[\sin\theta_v\cos\phi_v \quad \sin\theta_v\sin\phi_v \quad \cos\theta_v\right]^T, \quad (7.3\text{-}25)$$

For the two strongest clusters, say $n = 1$ and 2, rays are spread in delay to three sub-clusters (per cluster), with fixed delay offset {0,5,10 ns} (see Table 7.3-5). The delays of the sub-clusters are

$$\begin{aligned} \tau_{n,1} &= \tau_n + 0\,\text{ns} \\ \tau_{n,2} &= \tau_n + 5\,\text{ns} \\ \tau_{n,3} &= \tau_n + 10\,\text{ns} \end{aligned} \quad (7.3\text{-}26)$$

Twenty rays of a cluster are mapped to sub-clusters as presented in Table 7.3-5 below. The corresponding offset angles are taken from Table 7.3-3 with mapping of Table 7.3-5.

Table 7.3-5: Sub-cluster information for intra cluster delay spread clusters

sub-cluster #	mapping to rays	power	delay offset
1	1,2,3,4,5,6,7,8,19,20	10/20	0 ns
2	9,10,11,12,17,18	6/20	5 ns
3	13,14,15,16	4/20	10 ns

In the LOS case, define $H'_{u,s,n} = H_{u,s,n}$ and determine the channel coefficients by adding a single line-of-sight ray and scaling down the other channel coefficients generated by (7.3-22). The channel coefficients are given by:

$$H_{u,s,n}(t) = \sqrt{\frac{1}{K_R+1}} H'_{u,s,n}(t) + \delta(n-1)\sqrt{\frac{K_R}{K_R+1}} \begin{bmatrix} F_{rx,u,\theta}(\theta_{LOS,ZOA},\phi_{LOS,AOA}) \\ F_{rx,u,\phi}(\theta_{LOS,ZOA},\phi_{LOS,AOA}) \end{bmatrix}^T \begin{bmatrix} \exp(j\Phi_{LOS}) & 0 \\ 0 & -\exp(j\Phi_{LOS}) \end{bmatrix} \begin{bmatrix} F_{tx,s,\theta}(\theta_{LOS,ZOD},\phi_{LOS,AOD}) \\ F_{tx,s,\phi}(\theta_{LOS,ZOD},\phi_{LOS,AOD}) \end{bmatrix} . \exp\left(j2\pi \frac{\hat{r}^T_{rx,LOS} . \bar{d}_{rx,u}}{\lambda_0} \right) . \exp\left(j2\pi \frac{\hat{r}^T_{tx,LOS} . \bar{d}_{tx,s}}{\lambda_0} \right) . \exp\left(j2\pi \frac{\hat{r}^T_{rx,LOS} . \bar{v}}{\lambda_0} t \right) \quad (7.3\text{-}27)$$

where $\delta(\cdot)$ is the Dirac's delta function and K_R is the Ricean K-factor as generated in Step 4 converted to linear scale.

Step 12: Apply pathloss and shadowing for the channel coefficients.

Note that when multi-band simulation is needed, i.e., evaluating different frequencies for a certain BS-UT link at the same time, additional correlation modelling across different frequencies should be taken into account. To be specific, the propagation conditions generated in Step 2 (LOS states), the parameters generated in Step 4, the cluster delays and angles generated in Steps 5-7 are the same for all frequency bands. Other parameters and steps are independent for the frequency bands. Note that this additional correlation modelling applies for bands below 6GHz.

Table 7.3-6: Channel model parameters for 3D-UMi and 3D-UMa

Scenarios		3D-UMi			3D-UMa		
		LOS	NLOS	O2I	LOS	NLOS	O2I
Delay spread (DS) lgDS=$\log_{10}$(DS/1s)	$\mu_{\lg DS}$	-7.19	-6.89	-6.62	-7.03	-6.44	-6.62
	$\sigma_{\lg DS}$	0.40	0.54	0.32	0.66	0.39	0.32
AOD spread (ASD) lgASD=$\log_{10}$(ASD/1°)	$\mu_{\lg ASD}$	1.20	1.41	1.25	1.15	1.41	1.25
	$\sigma_{\lg ASD}$	0.43	0.17	0.42	0.28	0.28	0.42
AOA spread (ASA) lgASA=$\log_{10}$(ASA/1°)	$\mu_{\lg ASA}$	1.75	1.84	1.76	1.81	1.87	1.76
	$\sigma_{\lg ASA}$	0.19	0.15	0.16	0.20	0.11	0.16
ZOA spread (ZSA) lgZSA=$\log_{10}$(ZSA/1°)	$\mu_{\lg ZSA}$	0.60	0.88	1.01	0.95	1.26	1.01
	$\sigma_{\lg ZSA}$	0.16	0.16	0.43	0.16	0.16	0.43
Shadow fading (SF) [dB]	σ_{SF}	3	4	7	4	6	7
K-factor (*K*) [dB]	μ_K	9	N/A	N/A	9	N/A	N/A
	σ_K	5	N/A	N/A	3.5	N/A	N/A
Cross-Correlations	*ASD* vs *DS*	0.5	0	0.4	0.4	0.4	0.4
	ASA vs *DS*	0.8	0.4	0.4	0.8	0.6	0.4
	ASA vs *SF*	-0.4	-0.4	0	-0.5	0	0
	ASD vs *SF*	-0.5	0	0.2	-0.5	-0.6	0.2
	DS vs *SF*	-0.4	-0.7	-0.5	-0.4	-0.4	-0.5
	ASD vs *ASA*	0.4	0	0	0	0.4	0
	ASD vs *K*	-0.2	N/A	N/A	0	N/A	N/A
	ASA vs *K*	-0.3	N/A	N/A	-0.2	N/A	N/A
	DS vs *K*	-0.7	N/A	N/A	-0.4	N/A	N/A
	SF vs *K*	0.5	N/A	N/A	0	N/A	N/A
	ZSD vs *SF*	0	0	0	0	0	0
	ZSA vs *SF*	0	0	0	-0.8	-0.4	0
	ZSD vs *K*	0	N/A	N/A	0	N/A	N/A
	ZSA vs *K*	0	N/A	N/A	0	N/A	N/A
	ZSD vs *DS*	0	-0.5	-0.6	-0.2	-0.5	-0.6
	ZSA vs *DS*	0.2	0	-0.2	0	0	-0.2
	ZSD vs *ASD*	0.5	0.5	-0.2	0.5	0.5	-0.2
	ZSA vs *ASD*	0.3	0.5	0	0	-0.1	0
	ZSD vs *ASA*	0	0	0	-0.3	0	0
	ZSA vs *ASA*	0	0.2	0.5	0.4	0	0.5
	ZSD vs *ZSA*	0	0	0.5	0	0	0.5
Delay distribution		Exp	Exp	Exp	Exp	Exp	Exp
AoD and AoA distribution		Wrapped Gaussian			Wrapped Gaussian		
ZoD and ZoA distribution		Laplacian			Laplacian		
Delay scaling parameter r_τ		3.2	3	2.2	2.5	2.3	2.2
XPR [dB], see note 6	μ_{XPR}	9	8.0	9	8	7	9
	σ_{XPR}	3	3	5	4	3	5
Number of clusters N		12	19	12	12	20	12
Number of rays per cluster M		20	20	20	20	20	20
Cluster *ASD* (c_{ASD}) in [deg]		3	10	5	5	2	5
Cluster *ASA* (c_{ASA}) in [deg]		17	22	8	11	15	8
Cluster *ZSA* (c_{ZSA}) in [deg], see note 4		7	7	3	7	7	3
Per cluster shadowing std ζ [dB]		3	3	4	3	3	4
Correlation distance in the horizontal plane [m], see note 3	*DS*	7	10	10	30	40	10
	ASD	8	10	11	18	50	11
	ASA	8	9	17	15	50	17
	SF	10	13	7	37	50	7
	K	15	N/A	N/A	12	N/A	N/A
	ZSA	12	10	25	15	50	25
	ZSD	12	10	25	15	50	25

NOTE 1: *DS* = rms delay spread, *ASD* = rms azimuth spread of departure angles, *ASA* = rms azimuth spread of arrival angles, *ZSD* = rms zenith spread of departure angles, *ZSA* = rms zenith spread of arrival angles, *SF* = shadow fading, and *K* = Ricean K-factor.

NOTE 2: The sign of the shadow fading is defined so that positive SF means more received power at UT than predicted by the path loss model.

NOTE 3: The cross correlation values for *ZSD*, *ZSA* are based on WINNER+ and field measurements in sources WINNER+, R1-134221,R1-134222,R1-134795 , R1-131861 ,R1-132543, R1-132544, R1-133525 and adjustment is made to ensure positive definiteness.

NOTE 4: ZSA and cluster ZSA values are reused from Winner+.

NOTE 5: All large scale parameters are assumed to have no correlation between different floors.
This is assumed for simplicity due to lack of measurement results although it may not represent the reality.

NOTE 6: The value of XPR standard deviation for O2I 3D-UMi and O2I 3D-UMa is changed from 11 dB to 5 dB following the discussion in R1-150894.

NOTE 7: The following notation for mean ($\mu_{\lg X}$=mean{$\log_{10}$(X) }) and standard deviation ($\sigma_{\lg X}$=std{$\log_{10}$(X) }) is used for logarithmized parameters X.

Table 7.3-6a: Channel model parameters for 3D-InH

Scenarios		Indoor Hotspot	
		LOS	NLOS
Delay spread (DS) lgDS=$\log_{10}$(DS/1s)	$\mu_{\lg DS}$	–7.70	–7.41
	$\sigma_{\lg DS}$	0.18	0.14
AOD spread (ASD) lgASD=$\log_{10}$(ASD/1°)	$\mu_{\lg ASD}$	1.60	1.62
	$\sigma_{\lg ASD}$	0.18	0.25
AOA spread (ASA) lgASA=$\log_{10}$(ASA/1°)	$\mu_{\lg ASA}$	1.62	1.77
	$\sigma_{\lg ASA}$	0.22	0.16
ZOA spread (ZSA) lgZSA=$\log_{10}$(ZSA/1°)	$\mu_{\lg ZSA}$	1.22	1.26
	$\sigma_{\lg ZSA}$	0.23	0.67
Shadow fading (*SF*) [dB]	σ_{SF}	See Table 7.2-1	
K-factor (*K*) [dB]	μ_K	7	N/A
	σ_K	4	N/A
Cross-Correlations	ASD vs DS	0.6	0.4
	ASA vs DS	0.8	0
	ASA vs SF	–0.5	–0.4
	ASD vs SF	–0.4	0
	DS vs SF	–0.8	–0.5
	ASD vs ASA	0.4	0
	ASD vs *K*	0	N/A
	ASA vs *K*	0	N/A
	DS vs *K*	–0.5	N/A
	SF vs *K*	0.5	N/A
	ZSD vs SF	0.2	0
	ZSA vs SF	0.3	0
	ZSD vs K	0	N/A
	ZSA vs K	0.1	N/A
	ZSD vs DS	0.1	-0.27
	ZSA vs DS	0.2	-0.06
	ZSD vs ASD	0.5	0.35
	ZSA vs ASD	0	0.23
	ZSD vs ASA	0	-0.08
	ZSA vs ASA	0.5	0.43
	ZSD vs ZSA	0	0.42
Delay distribution		Exp	
AoD and AoA distribution		Laplacian	
ZoD and ZoA distribution		Laplacian	
Delay scaling parameter r_τ		3.6	3
XPR [dB]	μ_{XPR}	11	10
	σ_{XPR}	3	3
Number of clusters N		15	19
Number of rays per cluster M		20	20
Cluster ASD (c_{ASD}) in [deg]		5	5
Cluster ASA (c_{ASA}) in [deg]		8	11
Cluster ZSA (c_{ZSA}) in [deg]		9	9
Per cluster shadowing std ζ [dB]		6	3
Correlation distance in the horizontal plane [m]	DS	8	5
	ASD	7	3
	ASA	5	3
	SF	10	6
	K	4	N/A
	ZSA	4	4
	ZSD	4	4

NOTE 1: *DS* = rms delay spread, *ASD* = rms azimuth spread of departure angles, *ASA* = rms azimuth spread of arrival angles, *ZSD* = rms zenith spread of departure angles, *ZSA* = rms zenith spread of arrival angles, *SF* = shadow fading, and *K* = Ricean K-factor.

NOTE 2: The sign of the shadow fading is defined so that positive SF means more received power at UT than predicted by the path loss model.

NOTE 3: The following notation for mean ($\mu_{\lg X}$=mean{$\log_{10}$(X) }) and standard deviation ($\sigma_{\lg X}$=std{$\log_{10}$(X) }) is used for logarithmized parameters X.

Table 7.3-6b: Channel model parameters for 3D-RMa

Scenarios		Rural		
		LOS	NLOS	O2I
Delay spread (DS) lgDS=$\log_{10}$(DS/1s)	μ_{lgDS}	-7.49	-7.43	-7.47
	σ_{lgDS}	0.55	0.48	0.24
AOD spread (ASD) lgASD=$\log_{10}$(ASD/1°)	μ_{lgASD}	0.90	0.95	0.67
	σ_{lgASD}	0.38	0.45	0.18
AOA spread (ASA) lgASA=$\log_{10}$(ASA/1°)	μ_{lgASA}	1.52	1.52	1.66
	σ_{lgASA}	0.24	0.13	0.21
ZOA spread (ZSA) lgZSA=$\log_{10}$(ZSA/1°)	μ_{lgZSA}	0.47	0.58	0.93
	σ_{lgZSA}	0.40	0.37	0.22
Shadow fading (*SF*) [dB]	σ_{SF}	See Table 7.2-1		8
K-factor (*K*) [dB]	μ_K	7	N/A	N/A
	σ_K	4	N/A	N/A
Cross-Correlations	*ASD* vs *DS*	0	-0.4	0
	ASA vs *DS*	0	0	0
	ASA vs *SF*	0	0	0
	ASD vs *SF*	0	0.6	0
	DS vs *SF*	-0.5	-0.5	0
	ASD vs *ASA*	0	0	-0.7
	ASD vs *K*	0	N/A	N/A
	ASA vs *K*	0	N/A	N/A
	DS vs *K*	0	N/A	N/A
	SF vs *K*	0	N/A	N/A
Cross-Correlations [1)]	*ZSD* vs *SF*	0.01	-0.04	0
	ZSA vs *SF*	-0.17	-0.25	0
	ZSD vs *K*	0	N/A	N/A
	ZSA vs *K*	-0.02	N/A	N/A
	ZSD vs *DS*	-0.05	-0.10	0
	ZSA vs *DS*	0.27	-0.40	0
	ZSD vs *ASD*	0.73	0.42	0.66
	ZSA vs *ASD*	-0.14	-0.27	0.47
	ZSD vs *ASA*	-0.20	-0.18	-0.55
	ZSA vs *ASA*	0.24	0.26	-0.22
	ZSD vs *ZSA*	-0.07	-0.27	0
Delay distribution		Exp		
AoD and AoA distribution		Wrapped Gaussian		
ZoD and ZoA distribution		Laplacian		
Delay scaling parameter r_τ		3.8	1.7	1.7
XPR [dB]	μ_{XPR}	12	7	7
	σ_{XPR}	4	3	3
Number of clusters N		11	10	10
Number of rays per cluster M		20	20	20
Cluster ASD (c_{ASD}) in [deg]		2	2	2
Cluster ASA (c_{ASA}) in [deg]		3	3	3
Cluster ZSA (c_{ZSA}) in [deg]		2	2.5	3
Per cluster shadowing std ζ [dB]		3	3	3
Correlation distance in the horizontal plane [m] XPR [dB]	*DS*	50	36	36
	ASD	25	30	30
	ASA	35	40	40
	SF	37	120	120
	K	40	N/A	N/A
	ZSA	15	50	50
	ZSD	15	50	50

NOTE 1: *DS* = rms delay spread, *ASD* = rms azimuth spread of departure angles, *ASA* = rms azimuth spread of arrival angles, *ZSD* = rms zenith spread of departure angles, *ZSA* = rms zenith spread of arrival angles, *SF* = shadow fading, and *K* = Ricean K-factor.

NOTE 2: The sign of the shadow fading is defined so that positive SF means more received power at UT than predicted by the path loss model.

NOTE 3: The following notation for mean (μ_{lgX}=mean{$\log_{10}$(X) }) and standard deviation (σ_{lgX}=std{$\log_{10}$(X) }) is used for logarithmized parameters X.

Table 7.3-7: ZSD and ZoD offset parameters for 3D-UMa

Scenarios		3D-UMa	
		LOS	NLOS
ZOD spread (ZSD) lgZSD=$\log_{10}$(ZSD/1°)	μ_{lgZSD}	max[-0.5, -2.1(d_{2D}/1000) -0.01 (h_{UT} - 1.5)+0.75]	max[-0.5, -2.1(d_{2D}/1000) -0.01(h_{UT} - 1.5)+0.9]
	σ_{lgZSD}	0.40	0.49
ZoD offset	$\mu_{offset,ZOD}$	0	-10^{-0.62log10(max(10, d_{2D}))+1.93-0.07(h_{UT}-1.5)}
NOTE 1: The proposed average ESD is smaller than that of Winner+ NOTE 2: The ZSD parameters for O2I links are the same parameters that are used for outdoor links, depending on the LOS condition of the outdoor link part.			

Table 7.3-8: ZSD and ZoD offset parameters for 3D-UMi

Scenarios		3D-UMi	
		LOS	NLOS
ZOD spread (ZSD) lgZSD=$\log_{10}$(ZSD/1°)	μ_{lgZSD}	max[-0.5, -2.1(d_{2D}/1000)+0.01|h_{UT} - h_{BS}|+0.75]	max[-0.5, -2.1(d_{2D}/1000) +0.01max(h_{UT} - h_{BS},0) +0.9]
	σ_{lgZSD}	0.4	0.6
ZoD offset	$\mu_{offset,ZOD}$	0	-10^{-0.55log10(max(10, d_{2D}))+1.6}
NOTE 1: The proposed average ESD is smaller than that of Winner+ NOTE 2: The height dependence of ZOD offset observed from the ray-tracing data in R1-135765, R1-135999 and R1-135588 is not showing a common and strong trend. NOTE 3: The ZSD parameters for O2I links are the same parameters that are used for outdoor links, depending on the LOS condition of the outdoor link part.			

Table 7.3-9: ZSD and ZoD offset parameters for 3D-RMa

Scenarios		3D-RMa		
		LOS	NLOS	O2I
ZOD spread (ZSD) lgZSD=$\log_{10}$(ZSD/1°)	μ_{lgZSD}	max[-1, -0.17(d_{2D}/1000) -0.01(h_{UT} - 1.5) + 0.22]	max[-1, -0.19(d_{2D}/1000) -0.01(h_{UT} - 1.5) + 0.28]	max[-1, -0.19(d_{2D}/1000) -0.01(h_{UT} - 1.5) + 0.28]
	σ_{lgZSD}	0.34	0.30	0.30
ZoD offset	$\mu_{offset,ZOD}$	0	arctan((35 - 3.5)/d_{2D}) -arctan((35 - 1.5)/d_{2D})	arctan((35 - 3.5)/d_{2D}) -arctan((35 - 1.5)/d_{2D})

Table 7.3-10: ZSD and ZoD offset parameters for 3D-InH

Scenarios		3D-InH	
		LOS	NLOS
ZOD spread (ZSD) lgZSD=$\log_{10}$(ZSD/1°)	μ_{lgZSD}	1.02	1.08
	σ_{lgZSD}	0.41	0.36
ZoD offset	$\mu_{offset,ZOD}$	0	0

8 Simulations

Editor's note:: This clause includes baseline simulation results (corresponding to a number of antenna ports and transmission scheme supported by Rel-11) with the modified evaluation methodology

8.1 RSRP calculation formula

For channel model calibration and baseline performance evaluation, the following RSRP calculation formula for Tx antenna port p needed for UE attachment is used (applying $K_R = 0$ for NLOS UE). Note that the TX power is CRS transmitted power per RE. The notation below is according to equation (7.3-22). w_s (s=1, …, S) represents a complex weight vector used for virtualization of port p and U is the number of receive antenna elements.

$$RSRP_p = PL \cdot SF \cdot \sum_{u=1}^{U}\left(\left|\alpha_{0,u,p}\right|^2 + \sum_{n=1}^{N}\sum_{m=1}^{M}\left|\alpha_{n,m,u,p}\right|^2\right)\cdot\frac{TX_{power}}{U}, \quad (8.1\text{-}1)$$

where for NLOS path for n=1, …, N,

$$\alpha_{n,m,u,p} = \sqrt{\frac{P_n}{M\left(K_R+1\right)}}\begin{bmatrix} F_{rx,u,\theta}\left(\theta_{n,m,ZOA},\phi_{n,m,AOA}\right) \\ F_{rx,u,\phi}\left(\theta_{n,m,ZOA},\phi_{n,m,AOA}\right)\end{bmatrix}^T\begin{bmatrix} \exp\left(j\Phi_{n,m}^{\theta\theta}\right) & \sqrt{\kappa_{n,m}^{-1}}\exp\left(j\Phi_{n,m}^{\theta\phi}\right) \\ \sqrt{\kappa_{n,m}^{-1}}\exp\left(j\Phi_{n,m}^{\phi\theta}\right) & \exp\left(j\Phi_{n,m}^{\phi\phi}\right)\end{bmatrix}$$
$$\begin{bmatrix} F_{tx,p,\theta}\left(\theta_{n,m,ZOD},\phi_{n,m,AOD}\right) \\ F_{tx,p,\phi}\left(\theta_{n,m,ZOD},\phi_{n,m,AOD}\right)\end{bmatrix} \quad (8.1\text{-}2)$$

and for LOS path

$$\alpha_{0,u,p} = \sqrt{\frac{K_R}{K_R+1}}\begin{bmatrix} F_{rx,u,\theta}\left(\theta_{LOS,ZOA},\phi_{LOS,AOA}\right) \\ F_{rx,u,\phi}\left(\theta_{LOS,ZOA},\phi_{LOS,AOA}\right)\end{bmatrix}^T\begin{bmatrix} \exp\left(j\Phi_{LOS}\right) & 0 \\ 0 & -\exp\left(j\Phi_{LOS}\right)\end{bmatrix}\begin{bmatrix} F_{tx,p,\theta}\left(\theta_{LOS,ZOD},\phi_{LOS,AOD}\right) \\ F_{tx,p,\phi}\left(\theta_{LOS,ZOD},\phi_{LOS,AOD}\right)\end{bmatrix} \quad (8.1\text{-}3)$$

with

$$F_{tx,p,\theta}\left(\theta_{n,m,ZOD},\phi_{n,m,AOD}\right) = \sum_{s=1}^{S} w_s \exp\left(j2\pi\lambda_0^{-1}\left(\hat{r}_{tx,n,m}^T.\bar{d}_{tx,s}\right)\right)F_{tx,s,\theta}\left(\theta_{n,m,ZOD},\phi_{n,m,AOD}\right) \quad (8.1\text{-}4)$$

and

$$F_{tx,p,\phi}\left(\theta_{n,m,ZOD},\phi_{n,m,AOD}\right) = \sum_{s=1}^{S} w_s \exp\left(j2\pi\lambda_0^{-1}\left(\hat{r}_{tx,n,m}^T.\bar{d}_{tx,s}\right)\right)F_{tx,s,\phi}\left(\theta_{n,m,ZOD},\phi_{n,m,AOD}\right). \quad (8.1\text{-}5)$$

8.2 Simulation results

Geographical distance based and radio distance based wrapping methods R1-140842 [7] are used for simulations.
A different large scale parameter map (for generating correlated large-scale parameters from Table 7.3-6) is associated with each site including the wrapping candidate sites, e.g. 19x7=133 LSP maps for radio-distance based wrap or 61 LSP maps for geographical distance-based wrap can be used for a 19-site wrap-around.

The simulation results in this subclause are according to TR36.873 V12.0.0 – specifically, it is assumed that the XPR standard deviation in Table 7.3-6 for O2I 3D-UMi and O2I 3D-UMa cases is 11dB.

8.2.1 Phase-1 calibration

Phase-1 calibration results do not consider a fast-fading model.

Table 8.2-1: Simulation assumptions for phase-1 calibration

Parameter	Values
Scenarios	3D-UMa, 3D-UMi
Antenna configurations	config 1) K=M=10, with 0.5λ vertical antenna spacing config 2) K=1, M=1
Downtilt	102 degrees electrical tilt for antenna configuration 1
Handover margin (for calibration)	0dB
UE attachment	Based on pathloss considering LOS angle
Fast fading channel	Fast fading channel is not modelled
Wrapping method	1) Geographical distance based (mandatory) 2) Radio distance based (optional)
Metrics	1) Coupling loss – serving cell (based on LOS pathloss)
	2) Geometry (based on LOS pathloss)
	3) CDF of LOS EOD – serving cell

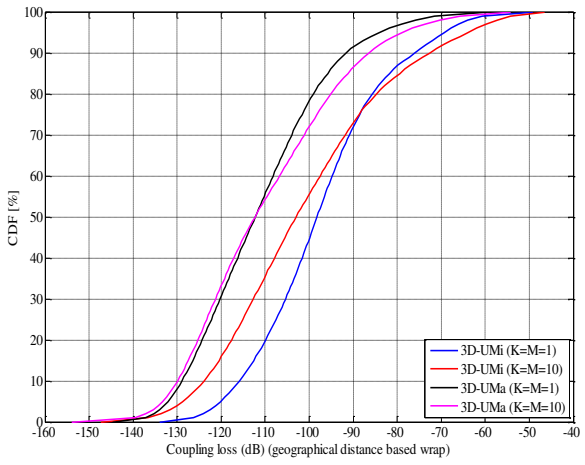

Figure 8.2-1: Coupling loss with geographical distance based wrap averaged over 18 sources (see R1-140843 [8])

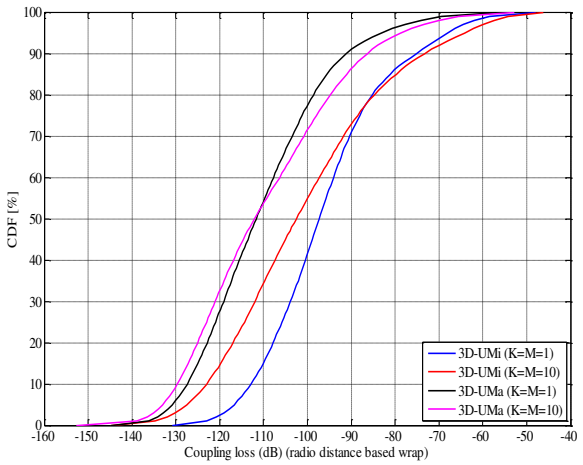

Figure 8.2-2: Coupling loss with radio distance based wrap averaged over 9 sources (see R1-140843 [8])

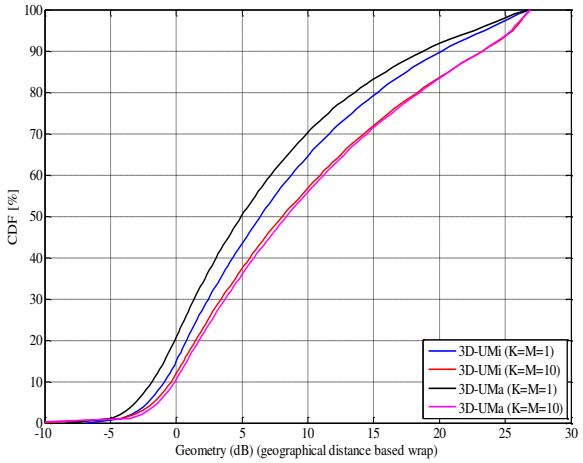

Figure 8.2-3: Geometry with geographical distance based wrap averaged over 18 sources (see R1-140843 [8])

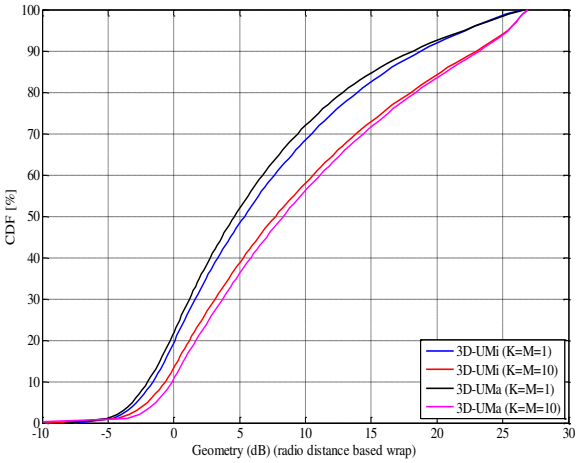

Figure 8.2-4: Geometry with geographical distance based wrap averaged over 9 sources (see R1-140843 [8])

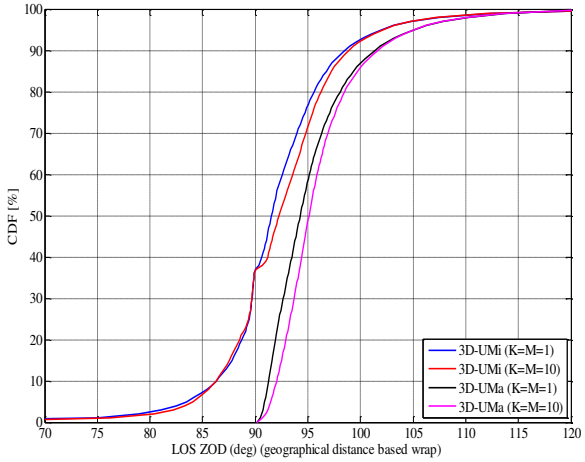

Figure 8.2-5: LOS ZOD with geographical distance based wrap averaged over 18 sources (see R1-140843 [8])

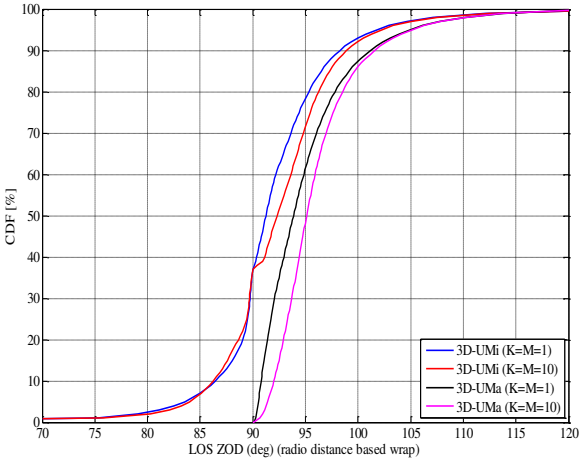

Figure 8.2-6: LOS ZOD with geographical distance based wrap averaged over 18 sources (see R1-140843 [8])

8.2.2 Phase-2 calibration

Table 8.2-2: Simulation assumptions for phase-2 calibration

Parameter	Values
Scenarios	3D-UMa, 3D-UMi
BS antenna configurations	Config 1: K=1, M=2, N=2, ULA, 0.5λ H/V spacing Config 2: K=M=10, N=2, X-pol (+/-45), 0.5λ H/V, θ_{etilt} = 102 degrees
BS port mapping	Config 1: the 4 antenna ports are mapped such that [0, 2; 1, 3] Config 2: the 4 antenna ports are mapped such that [0, 2, 1, 3] where 0/1 are -45 degree
MS antenna configurations	Config 1: 2 Rx ULA 0.5λ H spacing Config 2: 2Rx X-pol (0/+90)
System bandwidth	10MHz (50RBs)
UE attachment	Based on RSRP (formula) from CRS port 0
Carrier Frequency	2GHz
UE distribution	According to Table 6-1
Polarized antenna modelling	Model-1
UE array orientation	$\Omega_{UT,\alpha}$ uniformly distributed on [0,360] degree, $\Omega_{UT,\beta}$ = 90 degree, $\Omega_{UT,\gamma}$ = 0 degree
UE antenna pattern	Isotropic antenna gain pattern $A''(\theta'',\phi'')$ =1
Wrapping method	1) Geographical distance based (mandatory) 2) Radio distance based (optional)
Cluster elimination step 6	scaling factor not changed after cluster elimination
Handover margin (for calibration)	0 dB
Metrics	Wideband SINR before receiver – determined from RSRP (formula) from CRS port 0
	CDF of ZSD from the serving cell (according to circular angle spread definition of TR 25.996 [9] – Annex A and assuming an omni antenna pattern for $P_{n,m}$ determination)
	CDF of ZSA from the serving cell (according to circular angle spread definition of TR 25.996 [9] – Annex A and assuming an omni antenna pattern for $P_{n,m}$ determination)
	CDF of largest (1st) singular value (serving cell) in PRBs at t=0 plotted in 10*log10 scale
	CDF of smallest (2nd) singular value (serving cell) in PRBs at t=0 plotted in 10*log10 scale
	CDF of the ratio between the largest singular value and the smallest singular value (serving cell) in PRBs at t=0 plotted in 10*log10 scale
	CDF of coupling loss (serving cell)

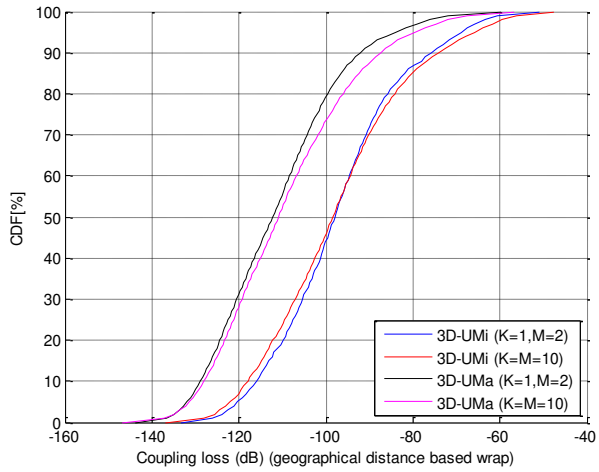

Figure 8.2-7: Coupling loss with geographical distance based wrap, median from 18 sources (see R1-143469 [10])

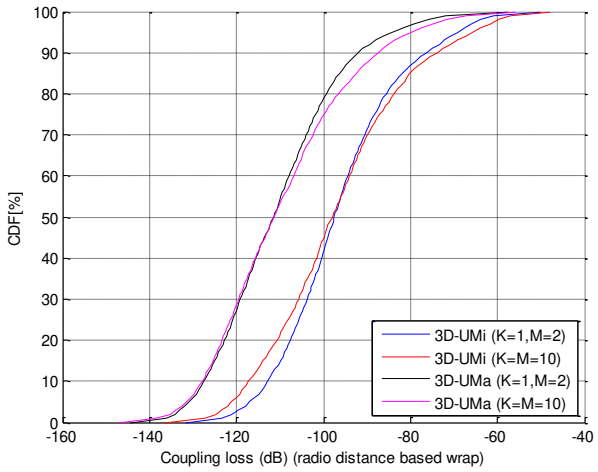

Figure 8.2-8: Coupling loss with radio distance based wrap, median from 7 sources (see R1-143469 [10])

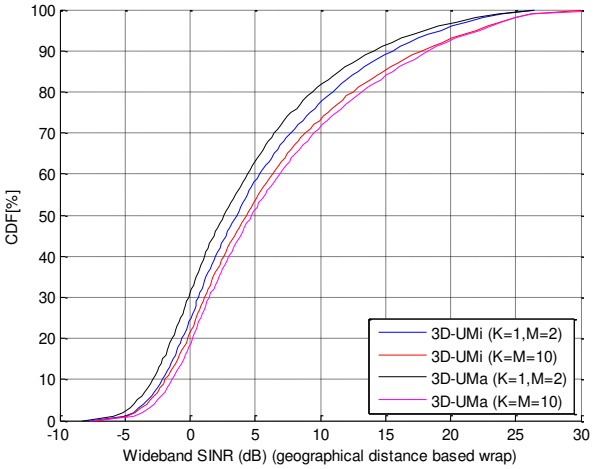

Figure 8.2-9: Wideband SINR with geographical distance based wrap, median from 21 sources (see R1-143469 [10])

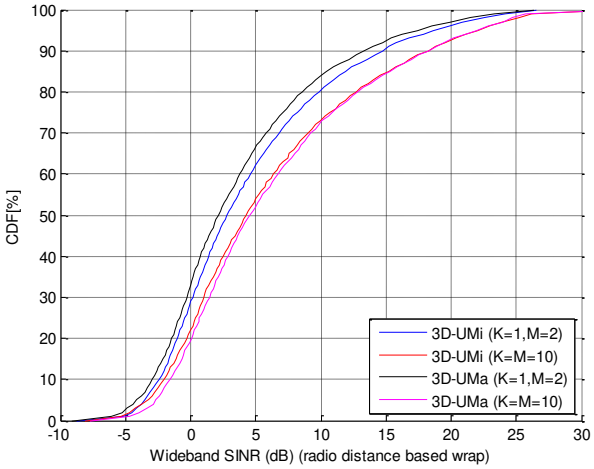

Figure 8.2-10: Wideband SINR with radio distance based wrap, median from 7 sources (see R1-143469 [10])

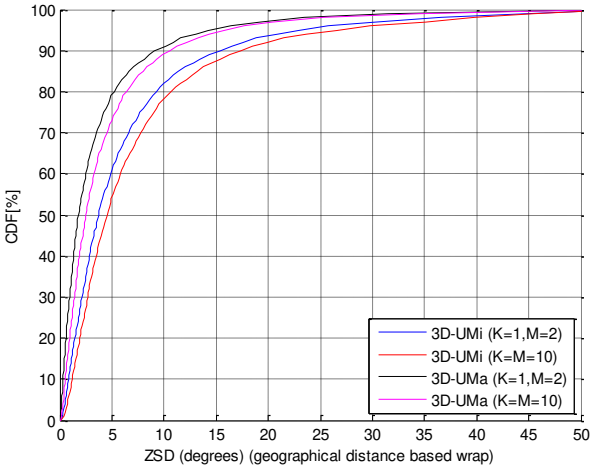

Figure 8.2-11: ZSD CDF with geographical distance based wrap, median from 21 sources (see R1-143469 [10])

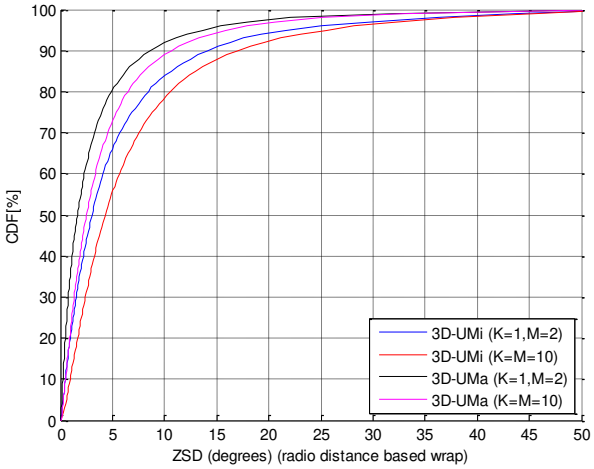

Figure 8.2-12: ZSD CDF with radio distance based wrap, median from 7 sources (see R1-143469 [10])

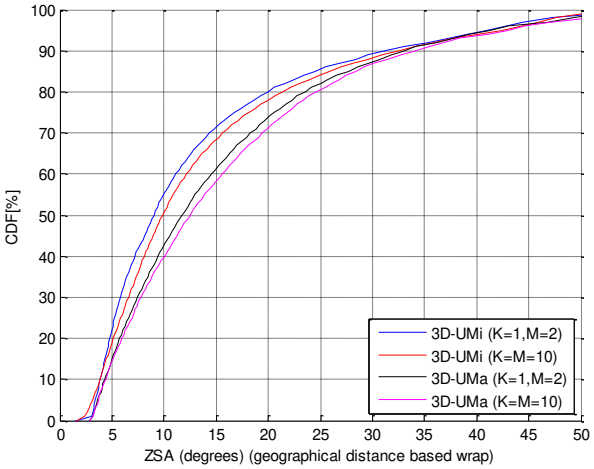

Figure 8.2-13: ZSA CDF with geographical distance based wrap, median from 21 sources (see R1-143469 [10])

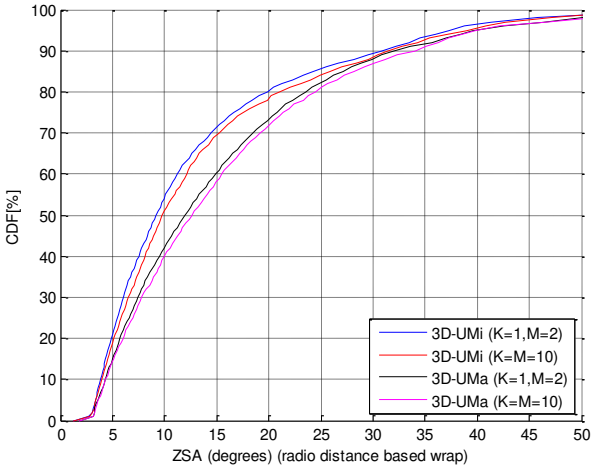

Figure 8.2-14: ZSA CDF with radio distance based wrap, median from 7 sources (see R1-143469 [10])

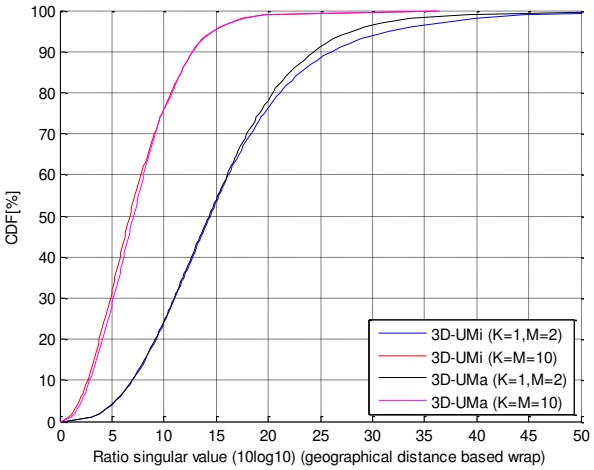

Figure 8.2-15: Ratio of singular values CDF with geographical distance based wrap, median from 21 sources (see R1-143469 [10])

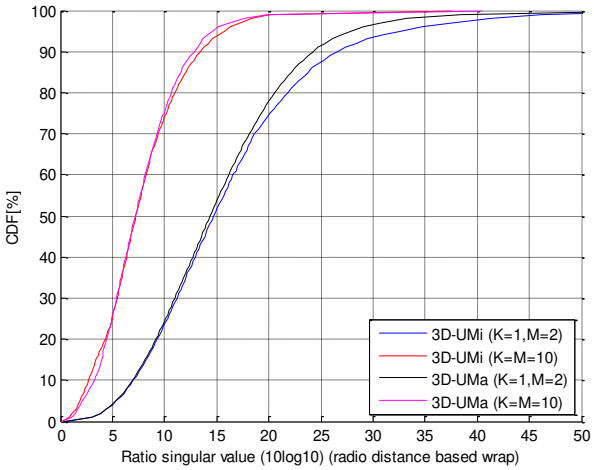

Figure 8.2-16: Ratio of singular values CDF with radio distance based wrap, median from 7 sources (see R1-143469 [10])

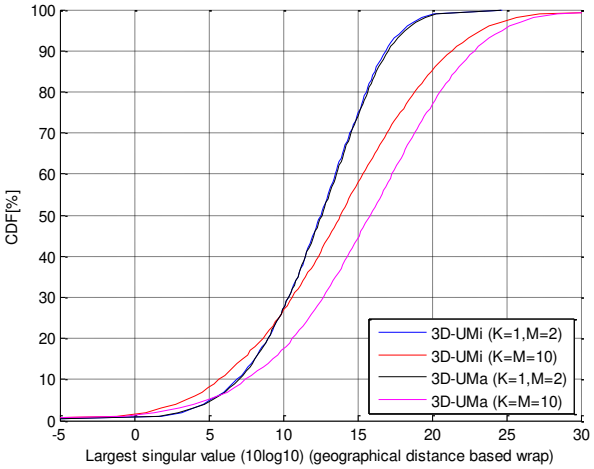

Figure 8.2-17: Largest singular value CDF with geographical distance based wrap, median from 21 sources (see R1-143469 [10])

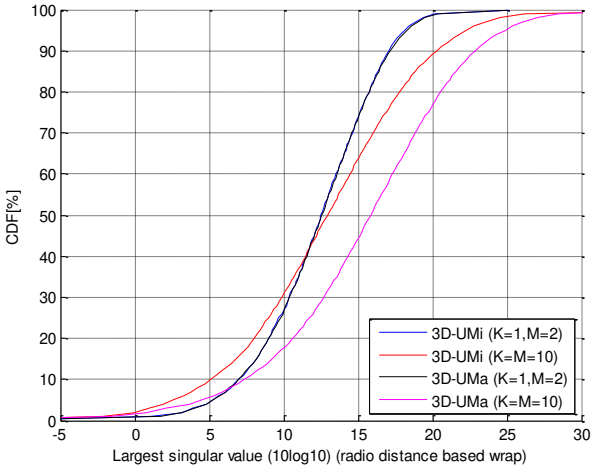

Figure 8.2-18: Largest singular value CDF with radio distance based wrap, median from 7 sources (see R1-143469 [10])

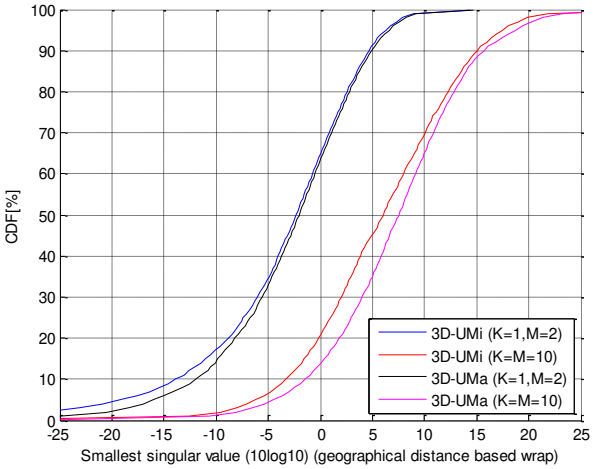

Figure 8.2-19: Smallest singular value CDF with geographical distance based wrap, median from 21 sources (see R1-143469 [10])

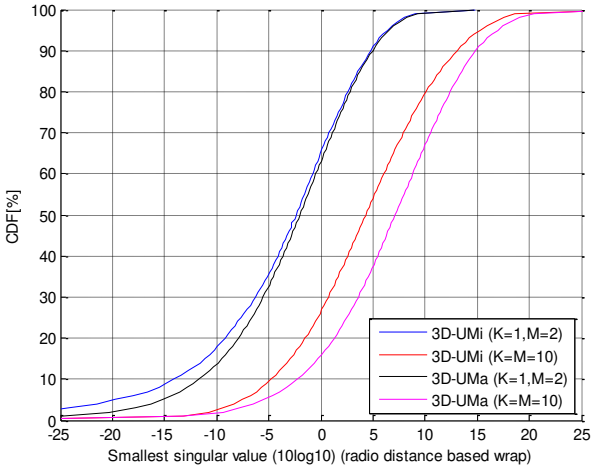

Figure 8.2-20: Smallest singular value CDF with radio distance based wrap, median from 7 sources (see R1-143469 [10])

8.2.3 Baseline calibration

Table 8.2-3: Simulation assumptions for baseline

Parameter	Values
Scenarios	3D-UMa, 3D-UMi
BS antenna configurations	K=M=10, N=2, X-pol (+/-45), 0.5λ H/V, θ_{etilt} = 102 degrees
BS port mapping	The 4 antenna ports are mapped such that [0, 2, 1, 3] where 0/1 are -45 degree
MS antenna configurations	2Rx X-pol (0/+90)
System bandwidth	10MHz (50RBs)
UE attachment	Based on RSRP (formula) from CRS port 0
Carrier Frequency	2GHz
Duplex	FDD
Network sync	Synchronized
Number of UEs per cell	10
UE distribution	According to Table 6-1
UE speed	3km/h
Polarized antenna modelling	1) Model-1 2) Model-2
UE array orientation	$\Omega_{UT,\alpha}$ uniformly distributed on [0,360] degree, $\Omega_{UT,\beta}$ = 90 degree, $\Omega_{UT,\gamma}$= 0 degree
UE antenna pattern	Isotropic antenna gain pattern $A''(\theta'',\phi'')$ =1
Wrapping method	1) Geographical distance based (mandatory) 2) Radio distance based (optional)
Cluster elimination step 6	scaling factor not changed after cluster elimination
Handover margin (for calibration)	0 dB
Traffic model	Full-buffer
Scheduler	PF, 1 UE per TTI allocation
Receiver	Ideal channel estimation
	Ideal interference modelling
	MMSE-IRC receiver
Interference model	Ideal interference from PDSCH which can be measured from IMR
Hybrid ARQ	Maximum 4 transmissions
Feedback	PUSCH 3-1
	CQI and PMI reporting triggered per 5ms
	Feedback delay is 5 ms
	Rel-8 4Tx codebook
Overhead	3 symbols for DL CCHs, 4 CRS ports and DM-RS with 12 REs per PRB
Transmission scheme	TM10, single CSI process, SU-MIMO with rank adaptation
Interference model	Ideal interference from PDSCH, can be measured from IMR
Metrics	Cell average SE
	5% cell-edge SE

Table 8.2-4: Baseline simulation results

Contribution number		R1-143030	R1-142908	R1-142869	R1-140423	R1-142859	R1-142992	R1-143111	R1-142936	R1-143199	R1-142970	R1-143232	R1-143237	R1-140767	R1-143144	R1-143257	R1-143120	Mean
3D-UMa - geo-dist, polarization model-1	avg SE	2.19	1.87	2.13	1.98	1.81	2.05	2.03	2.03	2.06	2.30	1.89		1.94	2.18	2.23	2.04	2.05
	5% SE	0.07	0.05	0.07	0.05	0.05	0.05	0.05	0.04	0.06	0.06	0.05		0.04	0.06	0.06	0.05	0.05
3D-UMa - geo-dist, polarization model-2	avg SE	2.20	1.91	2.06	1.95	1.79	1.99	1.97	1.97	2.07	2.28	1.88	2.00	1.94	2.18	2.24	2.04	2.03
	5% SE	0.07	0.05	0.06	0.05	0.04	0.05	0.05	0.04	0.06	0.06	0.04	0.06	0.04	0.06	0.06	0.05	0.05
3D-UMa - radio-dist, polarization model-1	avg SE		1.81	2.09		1.79	2.06			2.08				1.90	2.28			2.00
	5% SE		0.04	0.06		0.05	0.06			0.06				0.04	0.06			0.05
3D-UMa - radio-dist, polarization model-2	avg SE		1.87	2.06		1.75	1.99			2.09				1.91	2.28			1.99
	5% SE		0.04	0.05		0.04	0.05			0.05				0.04	0.06			0.05
3D-UMi - geo-dist, polarization model-1	avg SE	2.19	1.87	2.14	1.92	1.72	2.01	2.01	1.95	2.07	2.25	1.83		1.87	2.12	2.13	2.00	2.01
	5% SE	0.07	0.04	0.06	0.05	0.04	0.05	0.05	0.04	0.05	0.06	0.04		0.04	0.05	0.06	0.04	0.05
3D-UMi - geo-dist, polarization model-2	avg SE	2.20	1.90	2.09	1.88	1.71	1.96	1.96	1.89	2.08	2.23	1.83	1.92	1.88	2.12	2.15	2.00	1.99
	5% SE	0.07	0.05	0.05	0.04	0.04	0.05	0.05	0.04	0.05	0.06	0.04	0.05	0.04	0.05	0.06	0.04	0.05
3D-UMi - radio-dist, polarization model-1	avg SE		1.78	2.12		1.70	1.96			2.03				1.78	2.17			1.93
	5% SE		0.04	0.06		0.04	0.05			0.05				0.03	0.05			0.05
3D-UMi - radio-dist, polarization model-2	avg SE		1.80	2.08		1.66	1.91			2.05				1.79	2.17			1.92
	5% SE		0.04	0.05		0.04	0.05			0.05				0.03	0.05			0.05

Annex A: Change history

Change history							
Date	Meeting	TDoc	CR	Rev	Cat	Subject/Comment	New version
2013-01	RAN1#72	R1-130815				Initial draft	0.1.0
2013-04	RAN1#72 bis	R1-131244				Include agreements in RAN1#72 in clause 6	0.2.0
2013-05	RAN1#73	R1-132311				Include agreements in RAN1#72b in clause 6, 7	0.3.0
2013-08	RAN1#74	R1-134024				Include agreements and working assumptions in RAN1#72b, RAN1#73, RAN1#74 in clause 7	1.1.0
2013-08	RP-61	RP-131323	-	-		Submitted to RAN#61 for Information	1.0.0
2013-09	-	-	-	-		MCC clean-up	1.0.1
2013-10	RAN1#74 bis	R1-134980	-	-		Include agreements in RAN1#74 and RAN1#74bis	1.1.1
2013-11	RAN1#75	R1-136084				Include agreements in RAN1#75	1.2.0
2014-02	RAN1#76	R1-141062				Include agreements in RAN1#75 email discussions and RAN1#76	1.3.0
2014-03	RP-63	RP-140272				Submitted v130 to RAN#63 for approval	
2014-03	RP-63	RP-140423				MCC clean-up. Submitted v200 to RAN#63 for approval	2.0.0
2014-08	RAN1#78	R1-143663				Include agreements in RAN1#78	2.1.0
2014-09	RP-65	R1-141207				Approved by RAN#65 as Rel-12 version 12.0.0	12.0.0
2015-03	RP-67	R1-150362	0003	-		Change of XPR model standard deviation value and correction of sorting function for normalized delay	12.1.0
2015-06	RP-68	R1-150938	0004	-		Proposal on convention for 2D antenna element numbering	12.2.0
2016-12	RAN#74	RP-162370	0005	-	D	TR36.873_CR_Equation_Numbering	12.3.0
2016-12	RAN#74	RP-162370	0006	1	F	TR36.873_CR_Section_7.3	12.3.0
2016-12	RAN#74	RP-162370	0011	-	F	TR36.873 Section 5.1.3	12.3.0
2017-03	RAN#75	RP-170619	0012	-	F	CR to TR36.873 on rural channel model	12.4.0
2017-03	RAN#75	RP-170619	0013	-	F	TR36.873_CR_Scenarios	12.4.0
2017-03	RAN#75	RP-170619	0014	-	F	TR36.873_CR_Section_7.1	12.4.0
2017-03	RAN#75	RP-170619	0015	-	F	TR36.873_CR_Section_7.2	12.4.0
2017-03	RAN#75	RP-170619	0016	-	F	TR36.873_CR_Incorrect_Reference	12.4.0
2017-03	RAN#75	RP-170619	0017	-	F	TR36.873_CR_Align_LSP_Notation	12.4.0
2017-03	RAN#75	RP-170619	0018	-	F	TR36.873_CR_Notation_of_Cluster_Angular_Spreads	12.4.0
2017-03	RAN#75	RP-170619	0019	-	F	TR36.873_CR_Normalize_Cluster_Powers	12.4.0
2017-03	RAN#75	RP-170619	0020	-	F	TR36.873_CR_Incorrect_Reference_to_LSP_Table	12.4.0
2017-03	RAN#75	RP-170619	0021	-	F	TR36.873_CR_Adding_3D-InH_Scenario	12.4.0
2017-03	RAN#75	RP-170619	0022	-	F	CR on TR36.873 InH Scenario	12.4.0
2017-03	RAN#75	RP-170619	0023	-	F	Correction on multi-band modeling for TR36.873	12.4.0
2017-03	RAN#75	RP-170619	0024	-	F	Correction on ZSD parameter use in LoS O2I and NLoS O2I for TR38.873	12.4.0
2017-06	RAN#76	RP-171202	0025	-	F	Correction on site specific effective height for TR36.873	12.5.0
2017-06	RAN#76	RP-171202	0026	-	F	TR36.873_CR_Correction_on_Rural_LSP	12.5.0
2017-06	RAN#76	RP-171202	0027	-	F	TR36.873_CR_Correction_for_LOS_probability	12.5.0
2017-06	RAN#76	RP-171202	0028	-	F	TR36.873_CR_Scaling_factor_notation	12.5.0
2017-06	RAN#76	RP-171202	0029	-	F	TR36.873_CR_Notation_of_log-normal_distributed_random_variables	12.5.0
2017-06	RAN#76	RP-171202	0030	-	F	TR36.873_CR_Missing_LOS_Doppler	12.5.0
2017-07						MCC: UMa LOS probability in Table 7.2-2 is made fully visible	12.5.1
2017-09	RAN#77	RP-171643	0031	-	F	Correction on 3D-RMa channel model in TR 36.873	12.6.0
2017-09	RAN#77	RP-171643	0032	-	F	Correction on large scale parameters for 3D-InH in TR 36.873	12.6.0
2017-09	RAN#77	RP-171643	0033	2	F	Correction on cross polarization power ratios in TR 36.873	12.6.0
2017-12	RAN#78	RP-172683	0034	1	F	Correction on 3D-InH channel model in TR 36.873	12.7.0